

Isodensity Statistics on Clustering of High- z Objects in Cosmological Redshift-spaces

Atsushi Taruya¹ and Kazuhiro Yamamoto²

¹*Department of Physics, University of Tokyo, Tokyo 113-0033, Japan*

²*Department of Physics, Hiroshima University, Higashi-Hiroshima 739-8526, Japan*

ataruya@utap.phys.s.u-tokyo.ac.jp, kazuhiro@hiroshima-u.ac.jp

ABSTRACT

We discuss the systematic effects arising from the *cosmological redshift-space (geometric) distortion* on the statistical analysis of isodensity contour using high-redshift catalogs. Especially, we present a simple theoretical model for isodensity statistics in cosmological redshift-space, as a generalization of the work by Matsubara (1996). The statistical quantities considered here are the two- and three-dimensional genus of isodensity contour, the area of surface, the length of contour intersecting with a plane and the number of the crossing points of isodensity contour on a line. We give useful analytic formulae for the isodensity statistics, which take into account the corrections from the geometric distortion, the nonlinear clustering and the nonlinear velocity distortion phenomenologically. We then demonstrate how the geometric distortion and the nonlinear corrections alter shapes of the statistical quantities on the basis of plausible cosmological models. Our results show that the nonlinear correction can be sensitive to a choice of the redshift-space coordinate as increasing the redshift. The low-dimensional quantities such as two-dimensional genus systematically yield anisotropy due to the geometric and velocity distortions and their angle-dependence shows the 10 ~ 20% difference of amplitude. Sensitivity for typical high-redshift samples are estimated in an analytic manner, and the influence of the light-cone effect for the isodensity statistics is also discussed. A simple estimation suggests that the systematic effects of geometric and redshift-space distortions can become comparable or could be dominant to the statistical error of deep cluster samples and future high-redshift galaxy surveys. These systematic effects might be a useful tool in probing the cosmological model of our universe.

Subject headings: cosmology: theory - dark matter - large-scale structure of universe - galaxies : distances and redshifts - methods: statistical

1. Introduction

Recent observations of high-redshift objects have revealed dynamical aspects of the evolving universe. Measurements of Lyman-break galaxies provide evidences for the early galaxy assembly at the epoch $z \sim 3$, which put a serious constraint on the structure formation scenario (Steidal et al. 1998; Giavalisco et al. 1998). Clusters up to $z \sim 1$ have been observed, and the abundance suggests the universe with a low density parameter $\Omega \sim 0.3$ (e.g, Carlberg et al. 1997). Moreover, the upcoming wide-field surveys such as the Sloan Digital Sky Survey (SDSS) and the Two-Degree Field (2dF) survey promise to extend the observable scale of the universe and these enormous data will precisely reveal the clustering feature of the high-redshift quasars and galaxies. Since the analysis combining different redshift data sets has a potential to break the degeneracy of the cosmological parameters, as well as to provide the strong constraints on the structure formation scenario, statistical studies using the high-redshift objects are of great importance as a complementary to the measurements of cosmic microwave background anisotropy and the detection of cosmic shear.

Recently several authors have discussed various cosmological effects arising from proper observations of the high-redshift objects (e.g, Suto et al. 1999 and references therein). Apart from the biasing of the luminous objects, the main effects are summarized as follows:

1. geometric distortion : no one can obtain the correct three-dimensional map of the high-redshift objects without knowing the correct cosmological model of the universe. The uncertainty of the cosmological model may affect proper evaluation of the clustering pattern in the *cosmological redshift space* (Alcock & Paczyński 1979).
2. redshift-space distortion : peculiar motion of a cosmological object affects the estimation of the distance in a redshift survey, which causes the linear redshift-space distortion due to the bulk motion and the nonlinear velocity distortion due to the virialized random motion (finger-of-God effect) (Davis & Peebles 1983; Kaiser 1987; Suto & Sugimotohara 1991; Hamilton 1998 for a review).
3. light-cone effect : because an entire sample does not consist of objects on a constant-time hypersurface but on a light cone, the redshift evolution of the objects inevitably contaminates the data. Therefore, in a wide and deep survey, it becomes important to incorporate the light-cone effect into statistical quantities, for example, two-point correlation function and the power spectrum (Matarrese et al. 1997; Yamamoto & Suto 1999).

For the popular two-point statistics, the significance of these effects have been studied in detail and the robustness of the theoretical prediction is checked by the numerical simulation (Ballinger et al. 1996; Matsubara & Suto 1996; Magira et al. 2000; Hamana et al. 2000). Using the theoretical formulae, the feasibility of cosmological test with geometric distortion has been

investigated (Yamamoto, Nishioka & Taruya 2000). Further, the analysis is developed to the higher-order moments on a light-cone (Matsubara et al. 1997).

Here we extend these analyses to the isodensity statistics. That is, we investigate the influences of the above cosmological effects on the isodensity statistics, which have not been ever clarified. The isodensity statistics like the genus G_3 and area statistic N_3 have progressively become important as a quantitative measure of the topology of the large-scale structure. Analytical expressions of the isodensity statistics are derived for the Gaussian random field and some cases of non-Gaussian field in real space (e.g. Bardeen et al. 1986; Hamilton et al. 1986; Matsubara 1994, 2000; Matsubara & Yokoyama 1996). With these analytic formulae, the isodensity statistics computed from the redshift surveys of galaxies and/or the simulated dark matter catalogues are comprehensively understood (Colley et al. 2000 and references therein).

While most authors of these works have focused on the low-redshift objects except for the cosmic microwave background anisotropy, the analysis using the high-redshift samples is expected to provide an important clue on the origin and evolution of proto-galaxies and proto-clusters. In fact, Park et al. (2000) have recently analyzed the two-dimensional genus using the galaxies taken from the Hubble Deep Field and quantified the feature of early galaxy assembly. Remarkably, their samples are widely distributed over the redshift range $0 \lesssim z \lesssim 3$, which revealed an unprecedentedly deep view of galaxy clustering. Although the analysis is still limited to the projected density field because of the large error of photometric redshift, precise measurement of redshift will enable us to quantify the various isodensity statistics defined in the three-dimensional space, as well as the quantities in the one- and two-dimensional space in near future.

Practically, the observed distribution of high-redshift objects suffers from the cosmological effects, which should be correctly taken into account when comparing such data with theoretical prediction. Then naive but important questions are as follows: how the cosmological effects affect the statistical study of isodensity contour; whether these effects are observed as signal or noise. Purpose of this paper is to address these issues by using a simple theoretical formulae for the isodensity statistics, in which the cosmological effects are faithfully incorporated. Partially, the influence of the linear (redshift-space) distortion is investigated by Matsubara (1996), though the effect turns out to be small. In his paper the corrections from the nonlinear clustering and the nonlinear velocity distortion, which become influential on small length scales, are not investigated, and neither is the geometric distortion.

In this paper, we generalize the Matsubara’s results to those incorporating the geometric distortion effect and the nonlinear correction taking account of the smoothing effect. With the extended formulae, we examine how the geometric and redshift-space distortions affect the isodensity statistics qualitatively and quantitatively. We will show that the nonlinear effect can be important even for a case with large smoothing scale because the scaling effect of the geometric distortion causes apparent enhancement of the nonlinear effects, which depends on choice of the cosmological redshift space. In addition we also discuss the sampling noise and the effect of finite redshift depth

for typical high-redshift samples by using our extended formulae.

We organized the paper as follows. In section 2, the cosmological redshift-space coordinate is introduced, and the statistical quantities incorporating the nonlinear corrections are described. Then we consider the isodensity statistics in cosmological redshift space in section 3. Based on the analytic formulae for the Gaussian field in appendix A, we present a nonlinear model of isodensity statistics. After demonstrating predictions of the model, sensitivity of the isodensity statistics and the effect of the light-cone are discussed in section 4. The final section 5 is devoted to summary and conclusion.

2. Density field in cosmological redshift space

2.1. Redshift-space coordinate

We start with the standard form of Friedman-Robertson-Walker metric

$$ds^2 = -c^2 dt^2 + a^2(t) [dr^2 + f_K(r)^2 (d\theta^2 + \sin^2 \theta d\phi^2)], \quad (1)$$

where $f_K(r)$ is the comoving angular diameter distance given by

$$f_K(r) = \begin{cases} \sin(\sqrt{K} r)/\sqrt{K} & (K > 0) \\ r & (K = 0) \\ \sinh(\sqrt{-K} r)/\sqrt{-K} & (K < 0) \end{cases}, \quad (2)$$

with the spatial curvature K

$$K \equiv \left(\frac{H_0}{c}\right)^2 (\Omega_0 + \lambda_0 - 1), \quad (3)$$

and the comoving radial distance

$$r(z) = \int_0^z \frac{c dz'}{H(z')}; \quad H(z) = H_0 \sqrt{\Omega_0(1+z)^3 + (1 - \Omega_0 - \lambda_0)(1+z)^2 + \lambda_0}. \quad (4)$$

The quantities, Ω_0 , λ_0 , and H_0 , respectively, denote the density parameter, cosmological constant, and the Hubble parameter, at the present epoch $z = 0$.

Because we are interested in a redshift survey, suppose that we could only know radial distances of objects in terms of the redshift z and separations between pairs of objects in terms of the angular diameter distances. This means that the relation between the comoving real space and the observable redshift space inherently depends on an assumption of the cosmological model of the universe, and that the radial component of peculiar velocities of the objects apparently alters the distribution in the observed redshift space.

Hereafter, unless otherwise stated, we will assume that the sample of objects located in the range $z - dz$ and $z + dz$ with $dz \ll z$ whose angular separations are of the order of dz . Then, the

distant-observer approximation is entirely valid. Within this approximation, we consider the object located at $\mathbf{r} = (r_1, r_2, r_3)$ in the comoving real space. For definiteness, we choose the third-axis as the line-of-sight direction. Denoting the corresponding coordinate in the observed cosmological redshift space by $\mathbf{s} = (s_1, s_2, s_3)$, the relation between \mathbf{s} and \mathbf{r} is given by

$$\begin{aligned} s_1 &\equiv \frac{q_1}{c_\perp(z)} = \frac{r_1}{c_\perp(z)}, \\ s_2 &\equiv \frac{q_2}{c_\perp(z)} = \frac{r_2}{c_\perp(z)}, \\ s_3 &\equiv \frac{q_3}{c_\parallel(z)} = \frac{1}{c_\parallel(z)} \left(r_3 + \frac{1}{H(z)} v_3 \right), \end{aligned} \quad (5)$$

where v_3 is the line-of-sight component of the peculiar velocity field. The observed redshift space \mathbf{s} is obtained from the new coordinate system $\mathbf{q} = (q_1, q_2, q_3)$ divided by the dimensionless factors c_\perp and c_\parallel . Since we must assume a distance-redshift relation $s = s(z)$ to plot a map, the factors c_\perp and c_\parallel depend on the assumption of the cosmological redshift space. Frequently, one adopts $s = s_{\text{Hb}}(z)$, the radial-distance relation extrapolating the Hubble law, and/or $s = s_{\text{Ed}}(z)$, the relation in Einstein-de Sitter universe:

$$s_{\text{Hb}}(z) \equiv \frac{cz}{H_0}, \quad (6)$$

$$s_{\text{Ed}}(z) \equiv \frac{2c}{H_0} \left(1 - \frac{1}{\sqrt{1+z}} \right). \quad (7)$$

Then, the geometric factors become

$$c_\parallel(z) \equiv \frac{dr(z)}{ds(z)} = \frac{H_0}{H(z)}, \quad c_\perp(z) \equiv \frac{f_K(r(z))}{s(z)} = \left(\frac{H_0}{c} \right) \frac{f_K(r(z))}{z}, \quad (8)$$

for the case $s = s_{\text{Hb}}(z)$ (Matsubara & Suto 1996), and

$$c_\parallel(z) = \frac{H_0}{H(z)} (1+z)^{3/2}, \quad c_\perp(z) = \left(\frac{H_0}{c} \right) \frac{f_K(r(z))}{2(1-1/\sqrt{1+z})}, \quad (9)$$

for the case $s = s_{\text{Ed}}(z)$ (Ballinger et al. 1996), respectively.

2.2. Field correlations

Recall that the number density fluctuation of luminous objects is observed in the cosmological redshift space \mathbf{s} . We can evaluate the fluctuation $\delta^{(s)}(\mathbf{s})$ smoothed over the spherical radius R_s :

$$\begin{aligned} \delta^{(s)}(\mathbf{s}; R_s) &= \int d^3\mathbf{s}' W(\mathbf{s} - \mathbf{s}'; R_s) \delta^{(s)}(\mathbf{s}') \\ &= \int \frac{d^3\mathbf{k}_s}{(2\pi)^3} \hat{W}(k_s R_s) \hat{\delta}^{(s)}(\mathbf{k}_s) e^{-i\mathbf{k}_s \cdot \mathbf{s}}, \end{aligned} \quad (10)$$

where the quantities \hat{W} and $\hat{\delta}^{(s)}$ are the Fourier transform of the window function W and the density field $\delta^{(s)}$, respectively. \mathbf{k}_s is the Fourier vector corresponding to the \mathbf{s} -space. In this paper, we adopt the Gaussian window function, i.e., $\hat{W}(y) = \exp(-y^2/2)$. The density fluctuations defined in \mathbf{q} - and \mathbf{r} -space are merely related to $\delta^{(s)}$ through the transformation (5).

For our purpose, it is convenient to introduce the new field variables:

$$\eta_i \equiv \partial_i \delta^{(s)}, \quad \zeta_{ij} \equiv \partial_i \partial_j \delta^{(s)}; \quad (i, j = 1, 2, 3), \quad (11)$$

where ∂_i is the derivative with respect to the cosmological redshift-space coordinate s_i . Since correlation functions in the redshift space are inherently anisotropic for the special direction of the line-of-sight, the variance and the cross-moments of the variables (11) have the following non-vanishing quantities:

$$\langle [\delta^{(s)}]^2 \rangle = \sigma_0^2, \quad (12)$$

$$\langle [\eta_3]^2 \rangle = \sigma_{1,\parallel}^2, \quad \langle \eta_I \eta_J \rangle = \frac{\sigma_{1,\perp}^2}{2} \delta_{IJ} = - \langle \zeta_{IJ} \delta^{(s)} \rangle, \quad (13)$$

$$\langle \zeta_{IJ} \zeta_{KL} \rangle = \frac{\sigma_{2,\perp}^2}{24} (\delta_{IJ} \delta_{KL} + \delta_{IK} \delta_{JL} + \delta_{IL} \delta_{JK}), \quad (14)$$

where $\langle \dots \rangle$ denotes ensemble average over the smoothed density fields. Subscripts I and J run from 1 to 2. The quantities σ_0 , $\sigma_{1,\parallel}$, $\sigma_{1,\perp}$ and $\sigma_{2,\perp}$ are related to the power spectrum $P^{(\text{crd})}$, defined in the cosmological redshift space \mathbf{s} . Substitution of (10) into (12), (13) and (14) yields

$$\sigma_0^2(R_s) = \int \frac{d^3 \mathbf{k}_s}{(2\pi)^3} \hat{W}^2(k_s R_s) P^{(\text{crd})}(k_{s,\parallel}, k_{s,\perp}; z), \quad (15)$$

$$\sigma_{1,\parallel}^2(R_s) = \int \frac{d^3 \mathbf{k}_s}{(2\pi)^3} \hat{W}^2(k_s R_s) P^{(\text{crd})}(k_{s,\parallel}, k_{s,\perp}; z) k_{s,\parallel}^2, \quad (16)$$

$$\sigma_{1,\perp}^2(R_s) = \int \frac{d^3 \mathbf{k}_s}{(2\pi)^3} \hat{W}^2(k_s R_s) P^{(\text{crd})}(k_{s,\parallel}, k_{s,\perp}; z) k_{s,\perp}^2, \quad (17)$$

$$\sigma_{2,\perp}^2(R_s) = \int \frac{d^3 \mathbf{k}_s}{(2\pi)^3} \hat{W}^2(k_s R_s) P^{(\text{crd})}(k_{s,\parallel}, k_{s,\perp}; z) k_{s,\perp}^4, \quad (18)$$

with

$$k_s = \sqrt{k_{s,\parallel}^2 + k_{s,\perp}^2},$$

where $k_{s,\parallel}$ ($k_{s,\perp}$) denotes the wave number parallel(perpendicular) to the line-of-sight direction.

We notice that the power spectrum $P^{(\text{crd})}(k_{s,\parallel}, k_{s,\perp}; z)$ is written by the power spectrum defined in the \mathbf{q} -space, $P^{(s)}(k_{\parallel}, k_{\perp}; z)$, where, k_{\parallel} and k_{\perp} are respectively the line-of-sight and its orthogonal component of the Fourier vector corresponding to the \mathbf{q} -space. Using the facts that $k_{s,\parallel} = c_{\parallel} k_{\parallel}$ and $k_{s,\perp} = c_{\perp} k_{\perp}$, we obtain

$$P^{(\text{crd})}(k_{s,\parallel}, k_{s,\perp}) = \frac{1}{c_{\parallel} c_{\perp}^2} P^{(s)}\left(\frac{k_{s,\parallel}}{c_{\parallel}}, \frac{k_{s,\perp}}{c_{\perp}}\right). \quad (19)$$

Thus, all of the field correlations can be expressed in terms of the quantities defined in the \mathbf{q} -space:

$$\sigma_0^2(R_s) = \int \frac{d^3\mathbf{k}}{(2\pi)^3} \hat{W}^2(k R_{\text{eff}}) P^{(s)}(k_{\parallel}, k_{\perp}; z), \quad (20)$$

$$\sigma_{1,\parallel}^2(R_s) = c_{\parallel}^2(z) \int \frac{d^3\mathbf{k}}{(2\pi)^3} \hat{W}^2(k R_{\text{eff}}) P^{(s)}(k_{\parallel}, k_{\perp}; z) k_{\parallel}^2, \quad (21)$$

$$\sigma_{1,\perp}^2(R_s) = c_{\perp}^2(z) \int \frac{d^3\mathbf{k}}{(2\pi)^3} \hat{W}^2(k R_{\text{eff}}) P^{(s)}(k_{\parallel}, k_{\perp}; z) k_{\perp}^2, \quad (22)$$

$$\sigma_{2,\perp}^2(R_s) = c_{\perp}^4(z) \int \frac{d^3\mathbf{k}}{(2\pi)^3} \hat{W}^2(k R_{\text{eff}}) P^{(s)}(k_{\parallel}, k_{\perp}; z) k_{\perp}^4, \quad (23)$$

where $k = \sqrt{k_{\parallel}^2 + k_{\perp}^2}$. The quantity R_{eff} is related to the smoothing radius R_s :

$$R_{\text{eff}} = c_{\perp} R_s \sqrt{1 - \left(\frac{k_{\parallel}}{k}\right)^2 \left\{1 - \left(\frac{c_{\parallel}}{c_{\perp}}\right)^2\right\}}. \quad (24)$$

Note that the spherically symmetric smoothing in the \mathbf{s} -space corresponds to the anisotropic filtering in the \mathbf{q} -space in general cases with $c_{\parallel} \neq c_{\perp}$. This can be regarded as an effect of the geometric distortion on the one-point statistics, as well as the isodensity statistics.

Now we need a model for the power spectrum, $P^{(s)}(k_{\parallel}, k_{\perp}; z)$ (or $P^{(\text{crd})}$), including the redshift-space distortion and nonlinear clustering. Phenomenologically, but fairly accurate fitting form of the power spectrum has been recently proposed by several authors (Cole et al. 1995; Ballinger et al. 1996; Suto et al. 1999), and its validity is successfully confirmed by N-body simulation (Magira et al. 2000). Hereafter, we assume that the observed number density fluctuation is simply proportional to the mass density contrast by introducing the biasing factor b as the function of redshift

$$\delta^{(r)}(\mathbf{r}, z) = b(z) \delta_{\text{mass}}^{(r)}(\mathbf{r}, z), \quad (25)$$

in real space. Then the power spectrum of the observed density fluctuations is written as

$$P_{\text{nl}}^{(s)}(k_{\parallel}, k_{\perp}; z) = b^2(z) P_{\text{mass}}^{(r)}(k) [1 + \beta(z) \mu^2]^2 D[k\mu \sigma_{\text{P}}(z)], \quad (26)$$

where $P_{\text{mass}}^{(r)}(k)$ is the power spectrum of mass fluctuation in real space, σ_{P} denotes the peculiar velocity dispersion, and we defined $\mu \equiv k_{\parallel}/k$. The factor $[1 + \beta \mu^2]^2$ describes the linear theory of redshift-space distortion (Kaiser 1987) and β is obtained through the differentiation of the linear growth factor $D_+(z)$:

$$\beta(z) = \frac{1}{b(z)} \frac{d \ln D_+(z)}{d \ln a} \simeq \frac{1}{b(z)} \left[\Omega^{0.6}(z) + \frac{\lambda(z)}{70} \left(1 + \frac{\Omega(z)}{2}\right) \right], \quad (27)$$

with

$$\Omega(z) = \left(\frac{H_0}{H(z)}\right)^2 (1+z)^3 \Omega_0, \quad \lambda(z) = \left(\frac{H_0}{H(z)}\right)^2 \lambda_0. \quad (28)$$

The last term in (26) is the damping factor due to the finger-of-God effect:

$$D[x] = \frac{1}{1 + x^2/2}, \quad (29)$$

which corresponds to the assumption of the exponential form for the distribution function of the pair-wise peculiar velocity in real space. To be specific, in this paper, we adopt the fitting formulae of Peacock & Dodds (1996) and Mo et al. (1997) for the nonlinear mass power spectrum $P_{\text{mass}}^{(r)}(k)$ and the peculiar velocity dispersion σ_P , respectively. Then the field correlations, σ_0 , $\sigma_{1,\parallel}$, $\sigma_{1,\perp}$ and $\sigma_{2,\perp}$ can be computed through the definitions (20-23).

3. Isodensity statistics in cosmological redshift space

In this section, we consider simple theoretical models for isodensity statistics in cosmological redshift space. After describing definitions of the isodensity statistics, plausible nonlinear formulae are presented, based on the Gaussian results in appendix A. Influences of the nonlinear corrections and the geometric distortion are quantitatively examined in familiar cold dark matter cosmological models.

3.1. Definitions

First consider the three-dimensional genus curve. The genus G_3 is defined by $-1/2$ times the Euler characteristics of two-dimensional surfaces. The Euler number density is given by (number of holes) – (number of isolated regions). Equivalently, this can be expressed by (number of maxima) + (number of minima) – (number of saddle points) of the isodensity contour with respect to some fixed direction irrespective of the isotropy of the random field. At a given density threshold $\nu \equiv \delta^{(s)}/\sigma_0$, the genus G_3 is defined by (Bardeen et al. 1986)

$$G_3^{(s)}(\nu) = -\frac{1}{2} \left\langle \delta_D(\delta^{(s)} - \nu\sigma_0) \delta_D(\eta_1) \delta_D(\eta_2) |\eta_3| (\zeta_{11}\zeta_{22} - \zeta_{12}^2) \right\rangle, \quad (30)$$

where $\delta_D(\cdot)$ denotes the Dirac's delta-function.

Genus is also defined for a two-dimensional random field. Consider the field in a two-dimensional flat plane S and its isodensity contours. The two-dimensional genus G_2 can be computed by counting the number of the isolated high(low)-density regions surrounded by the isodensity contours (Melott et al. 1989). Notice that the quantity G_2 depends on a configuration of the plane S because the distortion induced by the geometric and peculiar velocity effects makes the random field anisotropy (Matsubara 1996). Denoting the angle between the line-of-sight direction and the plane S by θ (see Fig.1), the two-dimensional genus per unit area, G_2 , is

$$G_2^{(s)}(\nu, \theta) = -\frac{1}{2} \left\langle \delta_D(\delta^{(s)} - \nu\sigma_0) \delta_D(\eta_1) |\eta_2 \sin \theta + \eta_3 \cos \theta| \zeta_{11} \right\rangle. \quad (31)$$

Next consider the area statistic N_3 . This was proposed by Ryden (1988) and Ryden et al. (1989) as a complementary to the genus statistics. Given a density height ν , the quantity N_3 quantifies the mean surface area of the isodensity contours per unit volume :

$$N_3^{(s)}(\nu) = \left\langle \delta_D(\delta^{(s)} - \nu\sigma_0) \sqrt{\eta_1^2 + \eta_2^2 + \eta_3^2} \right\rangle. \quad (32)$$

For a homogeneous and isotropic random field, $N_3^{(s)}(\nu)$ equals $4/\pi$ times the mean length of the isodensity contour with same height ν per unit area on a flat plane and twice the mean number of the crossing points per unit length on a straight line, which we denote by N_2 and N_1 , respectively (Ryden 1988). In cosmological redshift space, these statistics obviously depend on the angle θ between the line-of-sight direction and the plane S or the line L (Fig.1). Therefore we need treat N_2 and N_1 , separately, which can be defined as

$$N_2^{(s)}(\nu, \theta) = \left\langle \delta_D(\delta^{(s)} - \nu\sigma_0) \sqrt{\eta_1^2 + (\eta_2 \sin \theta + \eta_3 \cos \theta)^2} \right\rangle, \quad (33)$$

$$N_1^{(s)}(\nu, \theta) = \left\langle \delta_D(\delta^{(s)} - \nu\sigma_0) |\eta_2 \sin \theta + \eta_3 \cos \theta| \right\rangle. \quad (34)$$

3.2. Modeling the nonlinear density field and isodensity statistics

Provided the distribution function for the field variables $\delta^{(s)}$, η_i and ζ_{ij} , the expressions for the isodensity statistics defined in previous subsection can be derived analytically. For the homogeneous but anisotropic Gaussian random fields, we easily obtain the simple analytic formulae (appendix A). The influence of geometric distortion is naturally incorporated into them.

The Gaussian results, however, are rather idealistic and cannot be used beyond the linear regime. Properly, we must take into account non-Gaussianity of the density distribution function developed by the gravitational clustering in the cosmological redshift space. Since no rigorous treatment of nonlinear evolution has been found, we need first adopt a reliable model of the distribution function $\mathcal{P}(\delta^{(s)}, \eta_i, \zeta_{ij})$. A class of models for the nonlinear density field have been discussed, whose statistical property is characterized by a monotonic function F (e.g, Coles & Jones 1991):

$$\delta^{(s)}(\mathbf{s}) = F[\phi(\mathbf{s})], \quad (35)$$

where the scalar field $\phi(\mathbf{s})$ is a Gaussian random variable with zero mean and the unit variance. In this case, it is easy to derive analytic expressions of isodensity statistics from the Gaussian results in appendix A. This is partially done by Matsubara & Yokoyama (1996) for the genus curve G_3 . We generalize their result to the other statistics G_2 , N_3 , N_2 and N_1 . In appendix C, assuming the functional form (35), the analytic formulae for isodensity statistics in the non-Gaussian case are presented, which are simply obtained by transformation of the Gaussian results.

The plausible functional form (35) for the nonlinear density distribution has been investigated by several numerical works. They showed that the probability density distribution of one-point

statistics can be empirically fitted by the log-normal distribution function to a good accuracy (Kofman et al. 1994; Bernardeau & Kofman 1995; Taylor & Watts 2000). This is also the case in the redshift space (Hui et al. 2000). Observationally, the log-normal distribution function has been used as a model of the galaxy distribution ever since Hubble (1934) (e.g, Hamilton 1985; Bouchet et al. 1993; Kofman et al. 1994). Hence, we might use the log-normal function as a good approximation for the actual observed distribution.

The log-normal distribution is characterized by

$$F(\phi) = \frac{1}{\sqrt{1 + \sigma_0^2}} \exp[\sigma_{\text{LN}} \phi] - 1, \quad (36)$$

where

$$\sigma_{\text{LN}}^2 = \ln(1 + \sigma_0^2). \quad (37)$$

Then we obtain the one-point distribution function

$$\mathcal{P}_{\text{LN}}(\delta^{(s)})d\delta^{(s)} = \frac{1}{\sqrt{2\pi}\sigma_{\text{LN}}} \exp\left[-\frac{\{\ln(1 + \delta^{(s)}) + \sigma_{\text{LN}}^2/2\}^2}{2\sigma_{\text{LN}}^2}\right] \frac{d\delta^{(s)}}{1 + \delta^{(s)}}, \quad (38)$$

and

$$F^{-1}(\nu\sigma_0) = \frac{\ln(1 + \nu\sigma_0) + \sigma_{\text{LN}}^2/2}{\sigma_{\text{LN}}}, \quad \langle F_{,\phi}(\phi)^2 \rangle_{\phi} = \sigma_{\text{LN}}^2(1 + \sigma_0^2). \quad (39)$$

Using (39) and (C2)-(C6), the analytic expressions for log-normal distribution are obtained as follows :

$$G_{3,\text{LN}}^{(s)}(\nu) = \frac{1}{4\pi^2(1 + \sigma_0^2)^{3/2}} \frac{\sigma_{1,\perp}^2 \sigma_{1,\parallel}}{\sigma_{\text{LN}}^3} \left[1 - \left\{ \frac{\ln(1 + \nu\sigma_0) + \sigma_{\text{LN}}^2/2}{\sigma_{\text{LN}}} \right\}^2 \right] \times \exp\left\{ -\frac{[\ln(1 + \nu\sigma_0) + \sigma_{\text{LN}}^2/2]^2}{2\sigma_{\text{LN}}^2} \right\}, \quad (40)$$

for the three-dimensional genus, and

$$G_{2,\text{LN}}^{(s)}(\nu, \theta) = \frac{1}{8\pi(1 + \sigma_0^2)} \left(\frac{\sigma_{1,\perp}}{\sigma_{\text{LN}}} \right)^2 \frac{\ln(1 + \nu\sigma_0) + \sigma_{\text{LN}}^2/2}{\sigma_{\text{LN}}} \times \exp\left\{ -\frac{[\ln(1 + \nu\sigma_0) + \sigma_{\text{LN}}^2/2]^2}{2\sigma_{\text{LN}}^2} \right\} L(\gamma, \theta), \quad (41)$$

for the two-dimensional genus. The quantities, N_3 , N_2 , and N_1 reduce to

$$N_{3,\text{LN}}^{(s)}(\nu) = \frac{1}{2\sqrt{\pi}(1 + \sigma_0^2)} \frac{\sigma_{1,\perp}}{\sigma_{\text{LN}}} \exp\left\{ -\frac{[\ln(1 + \nu\sigma_0) + \sigma_{\text{LN}}^2/2]^2}{2\sigma_{\text{LN}}^2} \right\} J(\gamma), \quad (42)$$

$$N_{2,\text{LN}}^{(s)}(\nu, \theta) = \frac{1}{2\sqrt{\pi}(1 + \sigma_0^2)} \frac{\sigma_{1,\perp}}{\sigma_{\text{LN}}} \exp\left\{ -\frac{[\ln(1 + \nu\sigma_0) + \sigma_{\text{LN}}^2/2]^2}{2\sigma_{\text{LN}}^2} \right\} K(\gamma, \theta), \quad (43)$$

$$N_{1,\text{LN}}^{(s)}(\nu, \theta) = \frac{1}{2\sqrt{\pi}(1 + \sigma_0^2)} \frac{\sigma_{1,\perp}}{\sigma_{\text{LN}}} \exp\left\{ -\frac{[\ln(1 + \nu\sigma_0) + \sigma_{\text{LN}}^2/2]^2}{2\sigma_{\text{LN}}^2} \right\} L(\gamma, \theta). \quad (44)$$

where the functions J , K and L are respectively given by (B1), (B2) and (B4) in Appendix B, and we introduced the distortion parameter γ given by

$$\gamma \equiv \sqrt{2} \frac{\sigma_{1,\parallel}}{\sigma_{1,\perp}}. \quad (45)$$

Notice that the parameter γ equals unity when $c_{\parallel} = c_{\perp} = 1$ and the power spectrum is isotropic $P^{(s)}(k_{\parallel}, k_{\perp}) = P^{(s)}(k)$ from equations (21) and (22). When the geometric distortion is effective, the factors c_{\parallel} and c_{\perp} are not equal to unity. Further, when the linear distortion or the finger-of-God effect is influential, the power spectrum is no longer isotropic. Thus the deviation of γ from unity quantifies the collected distortion effects, and represents anisotropies of the isodensity contours. As will be described in section 3.3, γ is affected by the three distortion effects: the geometric distortion, the linear distortion, and the finger-of-God effect. The linear distortion increases γ . On the contrary the finger-of-God effect decreases γ . As for the geometric distortion, this depends on the choice of cosmological redshift space $s(z)$ (see eqs.[21] and [22]). When we adopt $s = s_{\text{Hb}}(z)$, γ is decreased due to the geometric distortion. Conversely when adopting $s = s_{\text{Ed}}$, γ is increased. These features of the geometric distortion are based on the assumption that the real universe is the Lambda CDM model (see below). The strength of each distortion effect depends on smoothing scale and redshift, which yields the scale-/time-dependence of the value γ .

The above formulae state that the amplitude of the isodensity statistics depends on the geometric and the peculiar velocity effects, whose influences are characterized by the parameter γ . The sensitivity to those effects can be understood from the function J , K and L . In figure 2, we plot the normalized amplitude $J(\gamma)/J(1)$, $K(\gamma, \theta)/K(1, 0)$ and $L(\gamma, \theta)/L(1, 0)$ as the functions of distortion parameter γ . To show the angle dependence of the functions K and L , we plot the cases $\theta = 0$ (solid), $\pi/6$ (long-dashed), $\pi/3$ (short-dashed) and $\pi/2$ (dotted). Figure 2 suggests that the distortion effects may significantly affect the isodensity statistics, especially for the quantities described by the function $L(\gamma, \theta)$, i.e., G_2 and N_1 . In next subsection, we will clarify how γ is varied by the distortion effects at a quantitative level.

Before proceeding the analysis, it should be noted that isodensity statistics in terms of the volume fraction f defined by

$$f \equiv \int_{\nu}^{\infty} \frac{dx}{\sqrt{2\pi}} e^{-x^2/2}, \quad (46)$$

instead of the density threshold ν , has been conventionally used in order to compare the Gaussian results with non-Gaussian cases (e.g, Gott et al. 1989; Vogely et al. 1994; Canavezes et al. 1998). In fact, the isodensity statistics labeled by f remains unchanged under the transformation (35) in real space. In cosmological redshift space, however, the statistics cannot be entirely characterized by the volume fraction because of the anisotropy. Moreover, we intend to clarify influences of the distortion effects including the nonlinear correction. Therefore, we use the straightforward expressions labeled by the density threshold ν .

3.3. Results

Adopting the above nonlinear model, we now give a prediction for isodensity statistics in specific cold dark matter (CDM) cosmological models. In this paper, we consider two typical CDM models, in which the cosmological parameters are chosen as $(\Omega_0, \lambda_0, \sigma_8, h) = (1.0, 0.0, 0.6, 0.5)$ (SCDM model) and $(\Omega_0, \lambda_0, \sigma_8, h) = (0.3, 0.7, 1.0, 0.7)$ (LCDM model), where σ_8 , the top-hat mass fluctuation amplitude at $8h^{-1}\text{Mpc}$, is normalized by the cluster abundance (e.g, Kitayama & Suto 1997). For the unknown biasing factor, we use the time-evolving biasing model by Fry (1996). This model simply accounts for the redshift evolution of number density fluctuations in the case that the formation and merging process can be negligible. Denoting the amplitude of the biasing factor at present by b_0 , the linearized equation of continuity yields

$$b(z) = 1 + \frac{b_0 - 1}{D_+(z)}. \quad (47)$$

We fix the value $b_0 = 1.5$ for brevity.

The distortion parameters γ and the field correlation σ_0 are the most important parameters to understand behaviors of the shape of the isodensity statistics. Therefore we first analyze γ and σ_0 . Figures 3 and 4 show γ and σ_0 as the functions of the smoothing radius R_s . Figure 3 shows the case adopting the cosmological redshift space with $s = s_{\text{HB}}(z)$ (see eqs.[6] and [8]). The results are depicted for the LCDM model (*Upper-panel*) and the SCDM model (*Lower-panel*), though the two models show almost similar behaviors. In each model the results at $z = 1$ (*Left-panel*) and $z = 3$ (*Right-panel*) are shown.

On each panel the solid line plots the case all the effects are incorporated. Because the solid line corresponds to the case observed in the space \mathbf{s} , which is referred to 's-space' on the panel. The solid line shows that the distortion parameter γ (the clustering amplitude σ_0) gradually increases (decreases) as the smoothing scale R_s increases. To understand the importance of the nonlinear and the geometric distortion effects, we also plot the linear results neglecting the nonlinear correction (*dashed line*) and the case in absence of the geometric distortion (*dot-dashed line*), which are referred to 's-space(linear)' and 'q-space' on the panel, respectively. The latter case corresponds to the result obtained in the \mathbf{q} -space (see eq.[5]), which is the same result obtained in the \mathbf{s} -space with setting $c_{\parallel} = c_{\perp} = 1$.

By comparing the behaviors of the solid and the dot-dashed lines for γ on large smoothing scales, where the linear distortion and the geometric distortion are influential, it is apparent that the linear distortion increases γ and that the geometric distortion decreases γ . On the other hand the nonlinear correction becomes important on small scales (compare *solid* and *dashed* lines). It appears that the nonlinear effects cause more significant influence on the distortion parameter γ rather than the clustering amplitude σ_0 . This is because the finger-of-God effect compensates the gravitational nonlinear growth and the resultant σ_0 becomes almost same as the linear result. As for γ , since the finger-of-God effect dominates the linear velocity distortion on small scales, γ is significantly decreased. It is notable that the correction from nonlinear effects still remains non-

negligible even at the larger smoothing length $R_s \sim 20h^{-1}\text{Mpc}$ in the cosmological redshift space s_{Hb} . This behavior is caused from the scaling effect of the geometric distortion through the factors c_{\parallel} and c_{\perp} . Note also that the difference between the solid line and the dot-dashed line becomes significant at higher redshift $z = 3$, which also indicates the importance of the geometric distortion effect at the higher redshift.

Figure 4 shows another example, where the cosmological redshift space is chosen as $s = s_{\text{Ed}}(z)$ (see eqs.[7] and [9]). In contrast with the case $s = s_{\text{Hb}}(z)$ in Figure 3a, the geometric distortion increases γ and suppresses the amplitude σ_0 in the case of the LCDM model (*Upper-panel*). For the SCDM case, the results in \mathbf{s} -space exactly coincides with those in \mathbf{q} -space because the cosmological redshift space coincide with the comoving real space and the geometric distortion is absent. In both cases, correction from the nonlinear effects becomes negligible on the scales $R_s \gtrsim 8h^{-1}\text{Mpc}$ at high-redshift. This is also true irrespective of whether the cosmological model of the real space is spatially flat or open.

For comparison, in Figure 3 and 4, the case of no bias is also shown by setting $b(z) = 1$ (*dotted line*). This alternation does not change the qualitative behavior, however, we can see that γ and σ_0 are affected by the amplitude of the bias as follows. Increasing the amplitude of the biasing factor, γ is decreased, conversely σ_0 is increased. This effect could be more significant at higher redshift because of time-evolution of the bias.

In principle, behaviors of the isodensity statistics can be entirely understood from Figure 2, 3, and 4. As a demonstration, however, in Figure 5 we plot shape-dependence of the genus G_3 (*upper panels*) and G_2 (*lower panels*) as functions of the density height ν for the LCDM model. Figure 6 shows the area statistics N_3 (*upper panels*), N_2 (*middle panels*), and N_1 (*lower panels*). In both Figures 5 and 6, the cosmological redshift space $s = s_{\text{Hb}}(z)$ ($s = s_{\text{Ed}}(z)$) is chosen for the panels in the left (right) hand side of the figures. As is expected, the shape of the isodensity statistics is very sensitive to the choice of the cosmological redshift space. In the case $s = s_{\text{Hb}}(z)$, the significance of the nonlinear correction leads to asymmetric shapes of the isodensity statistics even at the large smoothing length $R_s \simeq 10h^{-1}\text{Mpc}$ and at high-redshift. The relative amplitude of G_2 and N_1 is sensitive to the angle θ , which might be a useful tool to determine the cosmological model of our universe as a simple geometric test (Alcock & Paczyński 1978; see Sec.5). On the other hand, in the case $s = s_{\text{Ed}}(z)$, all the statistics have nearly symmetric shape. This indicates that the Gaussian linear results could be a good approximation. Interestingly, at high-redshift $z = 3$, the relative amplitude of the isodensity statistics has the opposite θ -dependence in the case $s = s_{\text{Ed}}(z)$, compared to the one in the case $s = s_{\text{Hb}}(z)$. As the angle θ increases, the relative amplitude becomes smaller in the case $s = s_{\text{Ed}}(z)$ and conversely larger in the case $s = s_{\text{Hb}}(z)$ (c.f. *left- and right-panels*). This behavior comes from the difference of the value γ . For the smoothing length adopted here, $\gamma < 1$ in the case $s = s_{\text{Hb}}(z)$, while $\gamma > 1$ in the case $s = s_{\text{Ed}}(z)$ (Figures 3 and 4). This fact causes the opposite θ -dependence, as is easily deduced from Figure 2.

4. Discussion

The analysis in previous section shows that the anisotropy caused by the geometric and the velocity distortions systematically affect the amplitude of the one- and two-dimensional quantities with the fractional power by $10 \sim 20\%$. For the three-dimensional quantities G_3 and N_3 , the scaling effect by the geometric distortion enhances or reduces the nonlinearity. These results are qualitatively correct as long as a large number of samples are distributed within a narrow range of the redshift. In this section, for practical purpose, we focus on the following issues: detectability of these effects (subsection 4.1); influence of finite redshift range of samples, i.e, the light-cone effect (subsection 4.2).

4.1. Sensitivity

For quantitative study of high-redshift clustering, we must be careful for the Poisson noise and the sampling noise as the main statistical errors. This is not an exception for the case of isodensity statistics. While the sampling noise arises from finiteness of the sampling volume, the Poisson noise masks the isodensity statistics of underlying density fluctuations when the samples of cosmological objects are sparse and rare. In this subsection, to compare the errors with the systematic effects of geometric and redshift-space distortions, we roughly estimate both errors in an analytical manner, and investigate sensitivity of the isodensity statistics assuming typical high-redshift samples.

Let us first estimate the Poisson noise. For simplicity, we consider the isodensity statistics for the Gaussian random fields. The analytic formulae in Appendix A reveal that the amplitude of the isodensity statistics can be written in a general form :

$$\mathcal{G}_i^{(s)}(\nu) \propto \left[\frac{\langle k_s^2 \rangle}{3} \right]^{i/2}, \quad (48)$$

where $i = 3$ for G_3 , $i = 2$ for G_2 , and $i = 1$ for the area statistics, and we defined

$$\langle k_s^2 \rangle \equiv \frac{\int d^3 \mathbf{k}_s \hat{W}^2(k_s R_s) P^{(\text{crd})}(k_s) k_s^2}{\int d^3 \mathbf{k}_s \hat{W}^2(k_s R_s) P^{(\text{crd})}(k_s)}, \quad (49)$$

with the Gaussian window function $\hat{W}(y) = e^{-y^2/2}$. In the expression (48), we have simply ignored the anisotropy due to the redshift-space distortions.

The influence of the Poisson noise can be roughly evaluated as follows. The effect of the Poisson sampling is incorporated by adding the shot-noise power spectrum (e.g., Feldman, Kaiser & Peacock 1994)

$$P_{\text{shot}}^{(\text{crd})} = \frac{1}{n_s}, \quad (50)$$

where n_s is the mean number density of the observed high-redshift objects. Then we insert the following power spectrum $P^{(\text{crd})}(k_s)$ into equation (49),

$$P^{(\text{crd})}(k_s) = P_{\text{true}}^{(\text{crd})}(k_s) + P_{\text{shot}}^{(\text{crd})}, \quad (51)$$

where $P_{\text{true}}^{(\text{crd})}(k_s)$ means the spectrum free from the shot noise. By substituting equation (51) into (48), we can evaluate the ratio of $\mathcal{G}_i^{(s)}$ incorporating the Poisson term to the one neglecting it (Canavezes et al. 1998). Here we consider the case that the spectrum is given in the power law form $P_{\text{true}}^{(\text{crd})} \propto k^{-1}$ in the cosmological redshift space for simplicity. This yields the correlation function of the form

$$\xi^{(s)}(s) = \int \frac{d^3 \mathbf{k}_s}{(2\pi)^3} P_{\text{true}}^{(\text{crd})}(k_s) \frac{\sin(k_s s)}{k_s s} = \left(\frac{s}{s_0} \right)^{-2},$$

where s_0 is a correlation length. Then the ratio of $\mathcal{G}_i^{(s)}$ reduces to

$$\frac{\mathcal{G}_i^{(s)} + \Delta \mathcal{G}_i^{(s)}}{\mathcal{G}_i^{(s)}} = \left(\frac{1 + \frac{3}{8\pi^{3/2}} \frac{1}{n_s s_0^2 R_s}}{1 + \frac{1}{4\pi^{3/2}} \frac{1}{n_s s_0^2 R_s}} \right)^{i/2} \simeq \left(1 + \frac{1}{8\pi^{3/2}} \frac{1}{n_s s_0^2 R_s} \right)^{i/2}, \quad (52)$$

where the last line is valid as long as the contribution from the Poisson noise term is small compared with the dominant contribution from the Gaussian random field. Thus the quantity defined by

$$\left(\frac{S}{N} \right)_{\text{shot}} \equiv 8\pi^{3/2} n_s s_0^2 R_s \quad (53)$$

qualitatively gives signal-to-noise ratio resulting from the Poisson noise contribution.

On the other hand, in estimating the sampling noise, a reliable and robust method is the numerical technique of bootstrap re-sampling, which has been widely used in the observational/numerical study of genus statistics. Although analytical estimation of sampling noise is rather difficult task, we can roughly infer the influence of finite sampling effect from *number of resolution elements* N_{res} which provides a useful measure for the statistical power of isodensity statistics (Gott et al. 1989; Canavezes et al. 1998). For a given redshift range of the sample region $[z_{\text{min}}, z_{\text{max}}]$, we have

$$N_{\text{res}} = \frac{\frac{\Delta\Omega}{3} \{s^3(z_{\text{max}}) - s^3(z_{\text{min}})\}}{\frac{4\pi}{3} R_s^3}, \quad (54)$$

where $\Delta\Omega$ denotes a fixed solid angle. Gott et al. (1989) introduced this quantity to discuss the quality of data sets and argued that for a fractional accuracy of 25% in measuring the genus curve, a sample with $N_{\text{res}} = 100$ is required. For a measurement with high fractional accuracy of \sim few %, large number of resolution element $N_{\text{res}} > 10^3$ is necessary. Note that in a recent study of Point Source Catalogue Redshift Survey of *IRAS* galaxies, number of resolution element reaches more

than 300 (Canavezes et al. 1998). In this paper, we use the quantity N_{res} to estimate the influence of the sampling noise.

Table 1 summarizes the signal-to-shot noise ratio (53) and the number of resolution element (54) assuming the typical samples of cosmological objects, SDSS/2dF quasars, Lyman-break galaxies, and cluster samples. Here, we also list the SDSS/2dF galaxies as a representative low- z sample. Typical values of the correlation length s_0 and the mean number density n_s are adopted to evaluate $(S/N)_{\text{shot}}$. To compute the quantity N_{res} , we assume the cosmological redshift space $s = s_{\text{Ed}}(z)$ and set the solid angle $\Delta\Omega$ by π steradian for the SDSS/2dF galaxies, quasars and clusters, 0.25 square degree for the Lyman-break galaxies. From Table 1, it is clear that the SDSS/2dF galaxy redshift surveys unambiguously provide us high quality data preferable to an analysis of the isodensity statistics. For our interest of high-redshift samples, the cluster samples can be good objects for studying the isodensity statistics. The systematic cosmological effects can dominate the Poisson and the sampling noise, and may act as signal. As for the Lyman-break galaxies, while the high signal-to-noise ratio $(S/N)_{\text{shot}}$ could be attained, the sampling error can dominate the signal due to the narrow field of sample region. In an optimistic sense, this is not a problem when the wide-field samples are supplied. The photometric SDSS galaxies beyond $z \gtrsim 0.2$ might be a candidate of such samples if the redshifts of objects are precisely measured, although the redshift range will be shallower $z \lesssim 1$. On the other hand, the quasar samples would be rather sparse and the Poisson noise unfortunately dominates the signal, though the sampling error becomes negligible.

The above estimation of statistical errors might be rather optimistic and idealistic. We do not consider the selection effect and the boundary effect of the survey region. Further, we should be aware that strength of cosmological effects as well as the statistical errors also depend on the biasing of objects, which might be one of the most important obstacle in estimating the sensitivity. In a rigorous sense, we cannot give any conclusive statements until elaborating a more quantitative study using numerical simulation, however, we can say that the systematic effects of geometric and velocity distortions cannot be entirely negligible. The isodensity statistics on clustering of high-redshift objects will be measured from the cluster samples, in addition to the high- z galaxies from the future wide-field surveys.

4.2. Light-cone Effect

Table 1 suggests that observations of a large volume region is more desirable to reduce the sampling noise. In this case, the redshift range of the samples becomes large, and the influence of the light-cone effect will be important. Namely, the time-evolution of the distribution of the objects should be properly taken into account. The light-cone effect on the two-point correlation function and power spectrum is rigorously formulated by Yamamoto & Suto (1999) and the effect is extensively investigated in various cosmological situations (Nishioka & Yamamoto 1999, 2000; Yamamoto et al. 1999; Suto et al. 2000a, b).

Unlike the two-point statistics, which are computed from the pair-count of objects with a fixed separation, the isodensity statistics can be estimated from the pixelated density fields. This situation is similar to the analysis of the higher order moments using the count-in-cell method (Matsubara et al. 1997). In this case, as long as the distant-observer approximation is valid, the light-cone effect is supposed to be incorporated into the isodensity statistics as follows:

$$G_i^{(\text{LC})}(\nu) = \frac{\int_{z_{\min}}^{z_{\max}} dz \left(\frac{dV_c^{(i)}}{dz} \right) G_i^{(s)}(\nu; z) w(z)}{\int_{z_{\min}}^{z_{\max}} dz \left(\frac{dV_c^{(i)}}{dz} \right) w(z)}, \quad (55)$$

where $G_i^{(s)}(\nu; z)$ denotes the i -dimensional genus statistics at redshift z , $dV_c^{(i)}$ is the comoving volume element in i -dimensional (cosmological redshift) space, and $w(z)$ is a weight function. In general, the weight function $w(z)$ arising from the selection effect is determined so as to maximize the signal-to-noise ratio. As stated in Suto et al. (1999), the pixelated density field at z is corrected by multiplying the inverse of the selection function $\Phi(z)$ for the density fields and $w(z)$ can be set to unity for $z_{\min} < z < z_{\max}$, in principle. This is actually done when we compute the genus curves from the observational data (e.g, Canavezes et al. 1998). Hence, we simply set $w(z) = 1$. The formula (55) can also be applicable to the area statistics by replacing $G_i^{(s)}(\nu; z)$ with $N_i^{(s)}(\nu; z)$, the i -dimensional area statistics.

In the above expression (55), the range of the integration $[z_{\min}, z_{\max}]$ and the volume factor $dV_c^{(i)}$ should be determined depending on geometry of the survey depth for the three dimensional statistics, and also depending on configuration of a plane (line) underlying the density fields for the two (one) dimensional statistics. As an example, let us consider the case that samples are distributed in the range of the radial distance $s(z_{\min}) \leq s \leq s(z_{\max})$ within a fixed solid angle $\Delta\Omega$. In this case, the i -dimensional volume factor becomes

$$dV_c^{(i)} = s(z)^{i-1} ds(z) \Delta\Omega. \quad (56)$$

As a demonstration, in Figure 7, we plot the three-dimensional genus $G_3^{(\text{LC})}$ for the Lyman-break galaxies (lower panels) and the high-redshift clusters (middle panels) as typical high- z samples, and the SDSS/2dF galaxies (upper panels) as a reference. We adopted the parameters of the redshift range of the samples and the smoothing radius listed in Table 1. The left and right panels show the cases $s = s_{\text{Hb}}(z)$ and $s = s_{\text{Ed}}(z)$, respectively. For each panel, solid lines show the genus curves incorporating the light-cone effect, $G_3^{(\text{LC})}(\nu)$. On the other hand the dashed and dotted lines show the ones on a constant hypersurface at $z = z_{\min}$ and z_{\max} , i.e., $G_3^{(s)}(\nu; z_{\min})$ and $G_3^{(s)}(\nu; z_{\max})$, respectively. In the similar way, Figure 8 shows the two-dimensional genus $G_2^{(\text{LC})}$. In the case of the two-dimensional genus G_2 , the two-dimensional slice S embedded in a survey field is taken to be parallel to the line-of-sight direction, i.e., $\theta = 0$.

From Figures 7 and 8, we might regard that the light-cone effect is not significant for these samples. That is, as long as the samples listed in Table 1 are concerned, the light-cone effect on the

shapes of isodensity statistics is not so significant. This might be because we focused on the shape of the isodensity statistics normalized by the amplitude at the threshold $\nu = 0$ and/or $\nu = 1$, which is sensitive to probability distribution function of the random field, rather than that of the clustering amplitude. At a high-redshift and/or with a large smoothing radius, the probability distribution as a function of the threshold ν merely has the weak dependence of time. This consideration suggests that the light-cone effect becomes important for smoothing scales on a boundary between linear and nonlinear regimes, where the evolution of the probability distribution function can be drastic.

5. Conclusions

In the present paper, we have considered various observational effects on the isodensity statistics of high-redshift objects, and estimated their influences, as a generalization of the work by Matsubara (1996). We have presented a simple theoretical model incorporating the geometric distortion and the nonlinear correction arising from the gravitational growth and the finger-of-God effects, together with useful analytic formulae. From this theoretical model (40)–(44), we have demonstrated that the geometric distortion affects the shapes of the isodensity statistics and that the nonlinear correction can be sensitive to a choice of the redshift-space coordinate as increasing the redshift. Based on these results, we have briefly discussed the detectability of these effects by evaluating the shot-noise and the sampling noise contaminations. Furthermore, the influence of the light-cone effect has been investigated. The important conclusions are summarized:

1. When the cosmological redshift space $s = s_{\text{Hb}}(z)$ (eqs.[6] and [8]) is chosen, the nonlinear correction has an effect on the isodensity statistics for smoothing length larger $R_s \simeq 10h^{-1}\text{Mpc}$ even at the higher redshift $z \gtrsim 1$, where the isodensity statistics have asymmetric shapes. On the other hand, when the cosmological redshift space $s = s_{\text{Ed}}(z)$ (eqs.[7] and [9]) is chosen, the nonlinear correction turns out to be small and the linear theory of redshift-space distortions using the Gaussian results (A1), (A2) and (A3)-(A5) could be a good approximation for the large smoothing scales. In both cases, the geometric and velocity distortions cause the angle-dependence in the low-dimensional quantities, and the relative amplitude can be changed by $10 \sim 20\%$.
2. The Poisson sampling error is crucial for the sparse sampling of high-redshift objects like the (SDSS/2dF) quasars. The finiteness of the sampling volume might affect the precise measurement of isodensity statistics with Lyman-break galaxies. Though more quantitative estimation of statistical errors using numerical simulations is needed, however, the isodensity statistics can be tested using clusters and high- z galaxies from future wide-field surveys. For these samples, the cosmological effects can be comparable or could be dominant to the Poisson and the sampling noise.
3. For a sample that the survey volume is large and the cosmological objects are distributed in a wide range of redshift, the light-cone effect can be influential. However, we infer that the

light-cone effect has a weak influence on the isodensity statistics as long as the time evolution of the probability distribution function is not drastic, though this picture might depend on the evolution of the biasing factor.

Because the model presented here are quite simple, the predictions should be checked by numerical simulations. The prediction can also be sophisticated by using more reliable nonlinear models deduced from the simulations. Recent development of cosmological N-body simulation enables us to obtain the enormous large volume data over a few Gpc (Colberg et al. 2000). The larger data comparable to the Hubble volume size will provide us with chances of quantitative studies for the isodensity statistics, as well as the two-point statistics, in which the light-cone effect inevitably becomes important.

Combining our theoretical template with these simulations, various cosmological implications might be yielded. One of the most interesting application is the geometric test proposed by Alcock & Paczyński (1979). As we have seen in Sec.3.3, the geometric distortion makes the observed structures distorted and it causes deformation of the isodensity contour. Since this effect is sensitive to the distance-redshift relation, the anisotropy of isodensity statistics might be a useful tool in investigating cosmological models, as well as the anisotropy of two-point statistics (Yamamoto, Nishioka & Taruya 2000). The present theoretical formulae include useful tools for quantifying the geometric distortion, as well as for testing statistical nature of biased density fields. To address these issues, however, a more quantitative analysis should be developed.

The uncertainty of the biasing can be a critical issue to clarify the topological features of large-scale structure. Throughout the analyses, we have put the linear biasing ansatz (25) and the evolution of the biasing simply given by the model (47) neglecting the merging and formation processes. In more realistic situation, the biasing of luminous objects is nonlinear and stochastic (Dekel & Lahav 1999) and the merging and formation processes might alter the evolution of biasing (e.g, Somerville et al. 2000; Taruya et al. 2000). However, recent theoretical and numerical studies suggest that the linear biasing assumption (25) can be a good approximation even in the quasi-linear regime (Coles, 1993; Scherrer & Weinberg 1998; Matsubara 1999; Taruya & Suto 2000; Taruya et al. 2000). Therefore, in a qualitative sense, we believe that the present analyses would have revealed the generic feature of isodensity statistics on the observed high-redshift objects. As for the evolution of biasing, the theoretical prediction based on the Press-Schechter formalism gives the biasing factor for the dark halo distribution accurately (Mo & White 1996; Jing 1998; Sheth & Tormen 1999). Incorporating this evolution model into our analytic formulae can provide a powerful tool for quantifying the distribution of clusters of galaxies. In any way the isodensity statistics may probe a distinctive aspect of the biasing factor. This will be discussed elsewhere (Hikage, Taruya & Suto 2000, in preparation).

We thank Prof. Suto for useful discussion and critical comments, Prof. Matsubara for useful discussion. A.T. gratefully acknowledges support from a JSPS (Japan Society for the Promotion of

Science) fellowship. K.Y. thanks Prof. Kojima and Mr. Nishioka for useful comments. This work is supported by the Inamori foundation and in part by the Grants-in-Aid program (11640280) by the Ministry of Education, Science, Sports and Culture of Japan.

REFERENCES

- Alcock, C., & Paczyński, B. 1979, *Nature*, 281, 4
- Ballinger, W.H., Peacock, J.A., & Heavens, A.F. 1996, *MNRAS*, 282, 877
- Bardeen, J.M., Bond, J.R., Kaiser, N., & Szalay, A.S. 1986, *ApJ*, 304, 15
- Bernardeau, F., & Kofman, L. 1995, *ApJ*, 443, 479
- Bouchet, F.R., Strauss, M.A., Davis, M., Fisher, K.B., Yahil, A., & Huchra, J. 1993, *ApJ*, 417, 36
- Canavezes, A., et al. 1998, *MNRAS*, 297, 777
- Carlberg, R.G., Morris, S.L., Yee, H.K., & Ellingson, E. 1997, *ApJ*, 479, L19
- Colberg, J.M., et al. 2000, *astro-ph/0005259*
- Cole, S., Fisher, K.B., & Weinberg, D.H. 1995, *MNRAS*, 275, 515
- Coles, P., & Jones, B. 1991, *MNRAS*, 248, 1
- Coles, P. 1993, *MNRAS*, 262, 1065
- Colley, W., Gott, J.R., Weinberg, D.H., Park, C., & Berlind, A.A. 2000, *ApJ*, 529, 795
- Davis, M., & Peebles, P.J.E. 1983, *ApJ*, 267, 465
- Dekel, A., & Lahav, O. 1999, *ApJ*, 520, 24
- Feldman, H.A., Kaiser, N., & Peacock, J.A. 1994, *ApJ*, 426, 23
- Fry, J.N. 1996, *ApJ*, 461, L65
- Giavalisco, M., Steidel, C.C., Adelberger, K.L., Dickinson, M., Pettini, M., & Kellogg, M. 1998, *ApJ*, 503, 543
- Gott J.R., et al. 1989, *ApJ*, 340, 625
- Hamilton, A.J.S. 1985, *ApJ*, 292, L35
- Hamilton, A.J.S., Gott, J.R., & Weinberg, D. 1986, *ApJ*, 309, 1
- Hamilton, A.J.S. 1998, in *The Evolving Universe: Selected Topics on Large-Scale Structure and on the Properties of Galaxies*, ed. D.Hamilton (Kluwer:Dordrecht), 185
- Hamana, T., Colombi S., & Suto, Y. 2000, *A & A*, submitted (*astro-ph/0010287*)
- Hubble, E. 1934, *ApJ*, 79, 8

- Hui, L., Kofman, L., & Shandarin, S.F. 2000, *ApJ*, 537, 12
- Jing, Y.P. 1998, *ApJ*, 503, L9
- Kaiser, N. 1987, *MNRAS*, 227, 1
- Kitayama, T. & Suto, Y. 1997, *ApJ*, 490, 557
- Kofman, L., Bertschinger, E., Gelb, J.M., Nusser, A., & Dekel, A. 1994, *ApJ*, 420, 44
- Magira, H., Jing, Y.P., & Suto, Y. 2000, *ApJ*, 528, 30
- Matarrese, S., Coles, P., Lucchin, F., & Moscardini, L. 1997, *MNRAS*, 286, 115
- Matsubara, T. 1994, *ApJ*, 434, L43
- Matsubara, T. 1996, *ApJ*, 457, 13
- Matsubara, T., & Yokoyama, J. 1996, *ApJ*, 463, 409
- Matsubara, T., & Suto, Y. 1996, *ApJ*, 470, L1
- Matsubara, T., Suto, Y., & Szapudi, I. 1997, *ApJ*, 491, L1
- Matsubara, T. 1999, *ApJ*, 525, 543
- Matsubara, T. 2000, *ApJ*, submitted (astro-ph/0006269)
- Melott, A.L., Cohen, A.P., Hamilton, A.J.S., Gott III, J.R., & Weinberg, D.H. 1989, *ApJ*, 345, 618
- Mo, H., & White, S.D.M. 1996, *MNRAS*, 282, 347
- Nishioka, H., & Yamamoto, K. 1999, *ApJ*, 520, 426
- Nishioka, H., & Yamamoto, K. 2000, *ApJ*, in press (astro-ph/9911491)
- Mo, H.J., Jing, Y.P., & Börner, G. 1997, *MNRAS*, 286, 979
- Park, C., Gott, J.R., & Choi, Y.J. 2000, *ApJ*, submitted (astro-ph/0008353)
- Peacock, J.A., & Dodds, S.J. 1996, *MNRAS*, 280, L19
- Ryden, B.S. 1988, *ApJ*, 333, L41
- Ryden, B.S., Melott, A.L., Craig, D.A., Gott, J.R., Weinberg, D.H., Scherrer, R.J., Bhavsar, S.P., & Miller, J.M. 1989, *ApJ*, 340, 647
- Scherrer R.J., & Weinberg, D.H. 1998, *ApJ*, 504, 607
- Sheth, R.K., & Tormen, G. 1999, *MNRAS*, 308, 119

- Somerville, R.S., Lemson, G., Sigad, Y., Dekel, Al., Kauffmann, G., White, S.D.M. 2000, MNRAS, submitted (astro-ph/9912073)
- Steidel, C.C., Adelberger, K.L., Dickinson, M., Giavalisco, M., Pettini, M., & Kellogg, M. 1998, ApJ, 492, 428
- Suto, Y., Sugihara, T. 1991, ApJ, 370, L15
- Suto, Y., Magira, H., Jing, Y.P., Matsubara, T., & Yamamoto, K. 1999, Prog.Theor.Phys.Suppl., 133, 183
- Suto, Y., Magira, H., & Yamamoto, K. 2000a, PASJ, 52, 249 (astro-ph/9912367)
- Suto, Y., Yamamoto, K., Kitayama, T., & Jing, Y.P. 2000b, ApJ, 534, 551
- Taylor, A.N., & Watts, P.I.R. 2000, MNRAS, 314, 92
- Taruya, A., & Suto, Y. 2000, ApJ, 543, November 1 issue, in press (astro-ph/0004288)
- Taruya, A., Magira, H., Jing, Y.P., & Suto, Y. 2000, PASJ, submitted
- Vogely, M.S., Park, C., Geller, M.J., Huchra, J.P., & Gott, J.R. 1994, ApJ, 420, 525
- Yamamoto, K., & Suto, Y. 1999, ApJ, 517, 1
- Yamamoto, K., Nishioka, H., & Suto, Y. 1999, ApJ, 527, 488
- Yamamoto, K., Nishioka, H., & Taruya, A. 2000, MNRAS, submitted

A. Analytic formulae for Gaussian random field

In this appendix, we give the analytic formulae of isodensity statistics, which have been previously derived by Matsubara (1996). Although he only consider the case in absence of the geometric distortion (i.e, $c_{\parallel} = c_{\perp} = 1$) by imposing the assumption of linear redshift-space distortion, his results can be easily extended to those incorporating the geometric distortion in a rather formal way, without any approximation except for the random Gaussianity.

Let us suppose that the density field is homogeneous random Gaussian. In this case, the joint probability distribution function $\mathcal{P}(\delta^{(s)}, \eta_i, \zeta_{ij})$ is divided into $\mathcal{P}(\delta^{(s)}, \zeta_{ij})\mathcal{P}(\eta_i)$ regardless of the anisotropy. Final expression for the three dimensional genus (30) is immediately obtained by following similar calculations in the homogeneous and isotropic case (Bardeen et al. 1986; Hamilton et al. 1986). The resultant formula does not alter the shape of the genus as a function of ν . Only the amplitude is changed¹:

$$G_3^{(s)}(\nu) = \frac{1}{4\pi^2} \frac{\sigma_{1,\perp}^2 \sigma_{1,\parallel}}{\sigma_0^3} (1 - \nu^2) e^{-\nu^2/2}. \quad (\text{A1})$$

On the other hand, for the two-dimensional genus (31), by using the relations

$$\begin{aligned} & \left\langle \delta_D(\delta^{(s)} - \nu\sigma_0) \delta_D(\eta_1) \mid \eta_2 \sin \theta + \eta_3 \cos \theta \mid \zeta_{11} \right\rangle \\ & \quad = \left\langle \delta_D(\delta^{(s)} - \nu\sigma_0) \zeta_{11} \right\rangle \left\langle \delta_D(\eta_1) \mid \eta_2 \sin \theta + \eta_3 \cos \theta \mid \right\rangle, \\ & \left\langle \delta_D(\delta^{(s)} - \nu\sigma_0) \zeta_{11} \right\rangle = \frac{-1}{\sqrt{8\pi}} \left(\frac{\sigma_{1,\perp}}{\sigma_0} \right)^2 \nu e^{-\nu^2/2}, \end{aligned}$$

and

$$\left\langle \delta_D(\eta_1) \mid \eta_2 \sin \theta + \eta_3 \cos \theta \mid \right\rangle = \frac{1}{\sqrt{2\pi}} L(\gamma, \theta),$$

one obtains

$$G_2^{(s)}(\nu, \theta) = \frac{1}{8\pi} \left(\frac{\sigma_{1,\perp}}{\sigma_0} \right)^2 \nu e^{-\nu^2/2} L(\gamma, \theta), \quad (\text{A2})$$

where the function L is defined by (B4) in Appendix B. In the above expression, we defined the distortion parameter γ given by (see also eq.[45])

$$\gamma \equiv \sqrt{2} \frac{\sigma_{1,\parallel}}{\sigma_{1,\perp}}.$$

Similar to the case of the genus statistics, the area statistics, N_3 , N_2 , and N_1 are calculated using the probability functions being $\mathcal{P}(\delta^{(s)}, \eta_i) = \mathcal{P}(\delta^{(s)})\mathcal{P}(\eta_i)$, which is entirely characterized by

¹This has been partially shown by Matsubara (1996) in the case of the linear redshift distortion.

the field correlations (12) and (13). After some manipulations, one can obtain the final expressions:

$$N_3^{(s)}(\nu) = \frac{1}{2\sqrt{\pi}} \frac{\sigma_{1,\perp}}{\sigma_0} e^{-\nu^2/2} J(\gamma), \quad (\text{A3})$$

$$N_2^{(s)}(\nu, \theta) = \frac{1}{2\sqrt{\pi}} \frac{\sigma_{1,\perp}}{\sigma_0} e^{-\nu^2/2} K(\gamma, \theta), \quad (\text{A4})$$

$$N_1^{(s)}(\nu, \theta) = \frac{1}{2\sqrt{\pi}} \frac{\sigma_{1,\perp}}{\sigma_0} e^{-\nu^2/2} L(\gamma, \theta), \quad (\text{A5})$$

where L is the same function as defined in (A2) and the functions J and K are also defined in Appendix B by (B1) and (B2), respectively.

B. Expressions of $J(\gamma)$, $K(\gamma)$ and $L(\gamma)$

We here present explicit formulae for the functions J , K and L to describe the isodensity statistics for Gaussian random field (Appendix A). The functions J , K and L are defined by the ensemble average of the Gaussian random field η as follows:

$$\begin{aligned} J(\gamma) &\equiv \frac{\sqrt{2}}{\sigma_{1,\perp}} \langle \sqrt{\eta_1^2 + \eta_2^2 + \eta_3^2} \rangle, \\ K(\gamma, \theta) &\equiv \frac{\sqrt{2}}{\sigma_{1,\perp}} \langle \sqrt{\eta_1^2 + (\eta_2 \sin \theta + \eta_3 \cos \theta)^2} \rangle, \\ L(\gamma, \theta) &\equiv \frac{\sqrt{2}}{\sigma_{1,\perp}} \langle |\eta_2 \sin \theta + \eta_3 \cos \theta| \rangle, \end{aligned}$$

where the ensemble average $\langle \dots \rangle$ is evaluated according to the Gaussian probability distribution function

$$\mathcal{P}(\eta_i) d\eta_1 d\eta_2 d\eta_3 = \frac{1}{(2\pi)^{3/2} (\sigma_{1,\parallel} \sigma_{1,\perp}^2 / 2)} \exp \left[-\frac{\eta_1^2 + \eta_2^2}{\sigma_{1,\perp}^2} - \frac{\eta_3^2}{2\sigma_{1,\parallel}^2} \right] d\eta_1 d\eta_2 d\eta_3.$$

From straightforward calculations, we obtain the following formulae. Note that these formulae are also used to obtain the results for the parameterized non-Gaussian case if we replace the quantities η_i , $\sigma_{1,\parallel}^2$ and $\sigma_{1,\perp}^2$ with $\partial_i \phi$, $\langle [\partial_3 \phi]^2 \rangle_\phi$ and $\langle [\partial_\perp \phi]^2 \rangle_\phi$, respectively. (see Section 3.2 and Appendix C).

B.1. $J(\gamma)$

$$J(\gamma) = \int \frac{dx dy dz}{(2\pi)^{3/2}} e^{-(x^2+y^2+z^2)/2} \sqrt{x^2 + y^2 + \gamma^2 z^2}$$

$$= \sqrt{\frac{2}{\pi}} \frac{Q^2}{\gamma} \times \begin{cases} -\frac{1}{Q(1-Q)} - \frac{1}{2Q\sqrt{Q}} \ln \left| \frac{1-\sqrt{Q}}{1+\sqrt{Q}} \right| & ; (|\gamma| > 1) \\ -\frac{1}{Q(1-Q)} - \frac{1}{Q\sqrt{|Q|}} \tan^{-1} \left(\frac{1}{\sqrt{|Q|}} \right) & ; (|\gamma| < 1) \end{cases}, \quad (\text{B1})$$

where we define $Q = \gamma^2/(\gamma^2 - 1)$.

B.2. $K(\gamma, \theta)$

$$\begin{aligned} K(\gamma, \theta) &= \int \frac{dxdydz}{(2\pi)^{3/2}} e^{-(x^2+y^2+z^2)/2} \sqrt{x^2 + (y \sin \theta + \gamma z \cos \theta)^2}, \\ &= \begin{cases} \sqrt{\frac{2}{\pi}} \sqrt{1 + (\gamma^2 - 1) \cos^2 \theta} E \left(\sqrt{\frac{(\gamma^2 - 1) \cos^2 \theta}{1 + (\gamma^2 - 1) \cos^2 \theta}} \right) & ; (|\gamma| > 1) \\ \sqrt{\frac{2}{\pi}} E \left(\sqrt{(1 - \gamma^2) \cos^2 \theta} \right) & ; (|\gamma| < 1) \end{cases}, \quad (\text{B2}) \end{aligned}$$

where $E(k)$ is the complete elliptical integral of the second kind,

$$E(k) = \int_0^{\pi/2} d\phi \sqrt{1 - k^2 \sin^2 \phi}. \quad (\text{B3})$$

B.3. $L(\gamma, \theta)$

$$\begin{aligned} L(\gamma, \theta) &= \int \frac{dxdydz}{(2\pi)^{3/2}} e^{-(x^2+y^2+z^2)/2} |y \sin \theta + \gamma z \cos \theta| \\ &= \sqrt{\frac{2}{\pi}} |1 + (\gamma^2 - 1) \cos^2 \theta|^{1/2}. \quad (\text{B4}) \end{aligned}$$

C. Analytic results for the parameterized non-Gaussian case

In this appendix, we derive analytic expressions for the isodensity statistics with a non-Gaussian distribution whose statistical property is characterized by a monotonic function of the random field $\phi(\mathbf{s})$ (see eq.[35]). Since the field $\phi(\mathbf{s})$ is a Gaussian variable with the zero mean and the unit variance, the one-point distribution function of the density fluctuations $P(\delta^{(s)})$ becomes

$$\mathcal{P}(\delta^{(s)}) d\delta^{(s)} = \frac{1}{\sqrt{2\pi}} \frac{\exp \left\{ -\frac{1}{2} [F^{-1}(\delta^{(s)})]^2 \right\}}{|F_{,\phi}[F^{-1}(\delta^{(s)})]|} d\delta^{(s)}$$

$$= \frac{1}{\sqrt{2\pi}} e^{-\phi^2/2} d\phi. \quad (\text{C1})$$

Recall that the ensemble average with respect to the density field $\delta^{(s)}$ can be computed through the average with respect to the Gaussian field ϕ . Using the fact that the field variables η_i and ζ_{ij} can be written by

$$\begin{aligned} \eta_i &= F_{,\phi} \partial_i \phi, \\ \zeta_{ij} &= F_{,\phi} \partial_i \partial_j \phi + F_{,\phi\phi} \partial_i \phi \partial_j \phi, \end{aligned}$$

the final results are obtained :

$$\begin{aligned} G_3^{(s)}(\nu) &= -\frac{1}{2} \langle \delta_D[F(\phi) - \nu\sigma_0] \delta_D[F_{,\phi} \partial_1 \phi] \delta_D[F_{,\phi} \partial_2 \phi] |F_{,\phi} \partial_3 \phi| \\ &\quad \times \{ [F_{,\phi} \partial_1 \partial_1 \phi + F_{,\phi\phi} (\partial_1 \phi)^2] [F_{,\phi} \partial_2 \partial_2 \phi + F_{,\phi\phi} (\partial_2 \phi)^2] - [F_{,\phi} \partial_1 \partial_2 \phi + F_{,\phi\phi} \partial_1 \phi \partial_2 \phi]^2 \} \rangle_\phi \\ &= -\frac{1}{2} \langle \delta_D[\phi - F^{-1}(\nu\sigma_0)] \delta_D[\partial_1 \phi] \delta_D[\partial_2 \phi] |\partial_3 \phi| \{ (\partial_1 \partial_1 \phi)(\partial_2 \partial_2 \phi) - (\partial_1 \partial_2 \phi)^2 \} \rangle_\phi \\ &= \frac{1}{(2\pi)^2} \frac{\sigma_{1,\perp}^2 \sigma_{1,\parallel}}{\{ \langle F_{,\phi}(\phi)^2 \rangle_\phi \}^{3/2}} \{ 1 - [F^{-1}(\nu\sigma_0)]^2 \} \exp \left\{ -\frac{1}{2} [F^{-1}(\nu\sigma_0)]^2 \right\}. \end{aligned} \quad (\text{C2})$$

for the three-dimensional genus (see also Matsubara & Yokoyama 1996), where the ensemble average $\langle \dots \rangle_\phi$ is taken with respect to the field ϕ . For the two-dimensional genus, we have

$$\begin{aligned} G_2^{(s)}(\nu, \theta) &= -\frac{1}{2} \langle \delta_D[F(\phi) - \nu\sigma_0] \delta_D[F_{,\phi} \partial_1 \phi] |F_{,\phi}(\partial_2 \phi \sin \theta + \partial_3 \phi \cos \theta)| \\ &\quad \times [F_{,\phi} \partial_1 \partial_1 \phi + F_{,\phi\phi} (\partial_1 \phi)^2] \rangle_\phi \\ &= -\frac{1}{2} \langle \delta_D[\phi - F^{-1}(\nu\sigma_0)] \delta_D[\partial_1 \phi] |\partial_2 \phi \sin \theta + \partial_3 \phi \cos \theta| \partial_1 \partial_1 \phi \rangle_\phi \\ &= \frac{1}{8\pi} \frac{\sigma_{1,\perp}^2}{\langle F_{,\phi}(\phi)^2 \rangle_\phi} F^{-1}(\nu\sigma_0) \exp \left\{ -\frac{1}{2} [F^{-1}(\nu\sigma_0)]^2 \right\} L(\gamma), \end{aligned} \quad (\text{C3})$$

where γ is given by (45) and we have used the formula (B4) when taking the ensemble average with respect to the Gaussian field $\partial_i \phi$. As for the area statistics N_3 , N_2 and N_1 , repeating the similar calculations yields

$$N_3^{(s)}(\nu) = \frac{1}{2\sqrt{\pi}} \frac{\sigma_{1,\perp}}{\sqrt{\langle F_{,\phi}(\phi)^2 \rangle_\phi}} \exp \left\{ -\frac{1}{2} [F^{-1}(\nu\sigma_0)]^2 \right\} J(\gamma), \quad (\text{C4})$$

$$N_2^{(s)}(\nu, \theta) = \frac{1}{2\sqrt{\pi}} \frac{\sigma_{1,\perp}}{\sqrt{\langle F_{,\phi}(\phi)^2 \rangle_\phi}} \exp \left\{ -\frac{1}{2} [F^{-1}(\nu\sigma_0)]^2 \right\} K(\gamma), \quad (\text{C5})$$

$$N_1^{(s)}(\nu, \theta) = \frac{1}{2\sqrt{\pi}} \frac{\sigma_{1,\perp}}{\sqrt{\langle F_{,\phi}(\phi)^2 \rangle_\phi}} \exp \left\{ -\frac{1}{2} [F^{-1}(\nu\sigma_0)]^2 \right\} L(\gamma). \quad (\text{C6})$$

In deriving the above formulae, we have used the following relations,

$$\begin{aligned} \sigma_0^2 &= \langle F(\phi)^2 \rangle_\phi, \\ \sigma_{1,\parallel}^2 &= \langle F_{,\phi}(\phi)^2 \rangle_\phi \langle [\partial_3 \phi]^2 \rangle_\phi, \end{aligned}$$

and

$$\frac{\sigma_{1,\pm}^2}{2} = \langle F_{,\phi}(\phi)^2 \rangle_{\phi} \langle [\partial_J \phi]^2 \rangle_{\phi} , \quad (\text{C7})$$

where the subscript J runs from 1 to 2.

Table 1. High-redshift samples and signal-to-noise ratios of isodensity statistics. As a representative low- z sample, we also list the SDSS/2dF galaxy samples. Typical values from observations are adopted for the correlation length s_0 and the mean number density n_s . The smoothing length R_s is specifically chosen as $R_s = 2.5s_0$ except for the quasar samples, $R_s = 50h^{-1}\text{Mpc}$. Then signal-to-noise ratio $(S/N)_{\text{shot}}$ is evaluated from definition (53). Number of resolution element N_{res} is computed from (54) assuming the cosmological redshift space $s = s_{\text{Ed}}(z)$ and setting the solid angle of survey field $\Delta\Omega$ by π steradian (SDSS galaxies, quasars and clusters) or 0.25 square degree (Lyman-break galaxies).

samples	$[z_{\text{min}}, z_{\text{max}}]$	$s_0[h^{-1}\text{Mpc}]$	$R_s[h^{-1}\text{Mpc}]$	$n_s[h^3\text{Mpc}^{-3}]$	$(S/N)_{\text{shot}}$	N_{res}
SDSS/2dF galaxies	[0.0, 0.2]	4.0	10	0.1	710	3.6×10^4
Clusters	[0.0, 2.0]	20.0	50	10^{-5}	9.0	3.3×10^4
Lyman-break galaxies	[2.0, 4.0]	4.0	10	10^{-2}	360	1.2×10^2
SDSS/2dF quasars	[0.0, 3.0]	4.0	50	10^{-6}	0.04	5.4×10^4

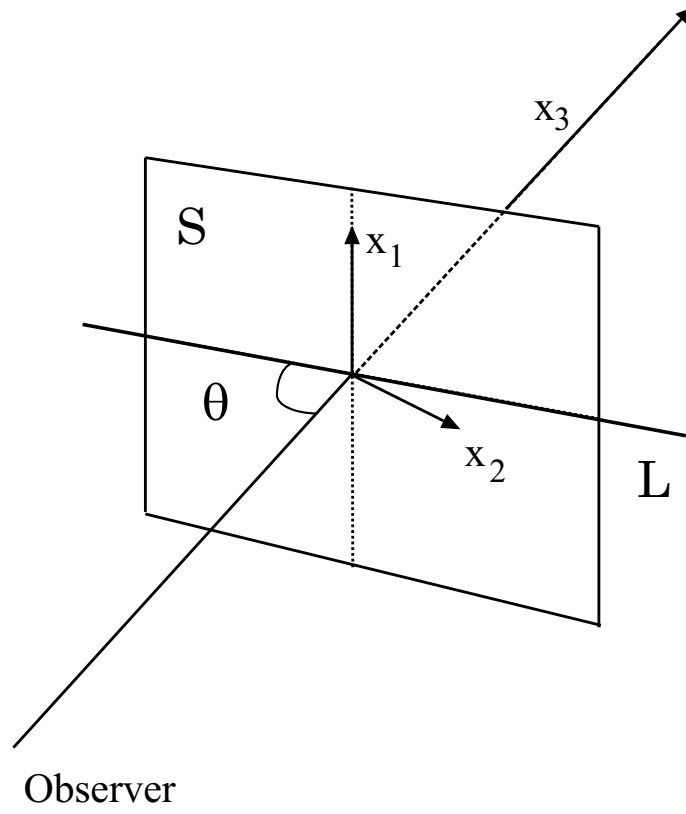


Fig. 1.— A sketch of cosmological redshift coordinate and the configuration of survey region (plane S /line L)

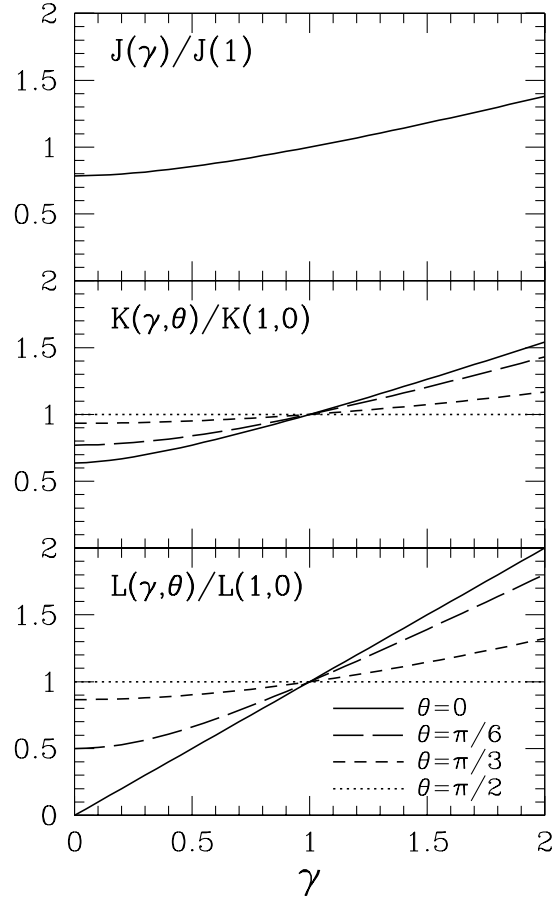


Fig. 2.— The normalized amplitude of J (*Upper*), K (*Middle*), and L (*Lower*) as the function of the distortion parameter γ (see also Appendix A). For K and L we fixed $\theta = 0$ (solid), $\pi/6$ (long-dashed), $\pi/3$ (short-dashed), and $\pi/2$ (dotted).

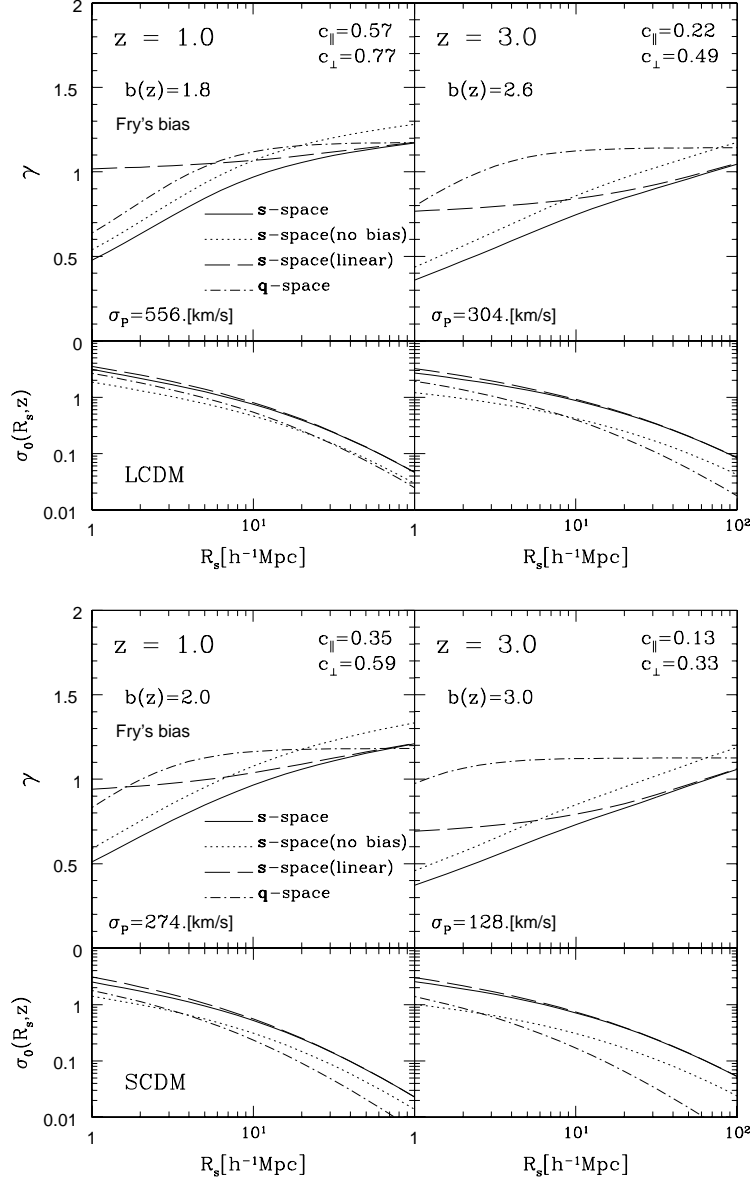


Fig. 3.— The scale-dependence of distortion parameter γ and the field correlation σ_0 as the function of the smoothing radius R_s in the case adopting the cosmological redshift space $s = s_{\text{Hb}}(z)$ (see eqs.[6] and [8]). *Upper-panels(Lower-panels)* show the LCDM (SCDM) model. The left (right) panel shows the case $z = 1$ ($z = 3$). Here, we used the biasing parameter given by (47) specifying the present value $b_0 = 1.5$. The solid and dot-dashed lines indicate the predictions from the nonlinear power spectrum (26), where the latter case is obtained by setting $c_{\parallel} = c_{\perp} = 1$. The dashed line shows the linear prediction, in which only the linear distortion and the geometric effect are taken into account. For comparison, we plot the result for the no-biasing case, $b(z) = 1$ (dotted line).

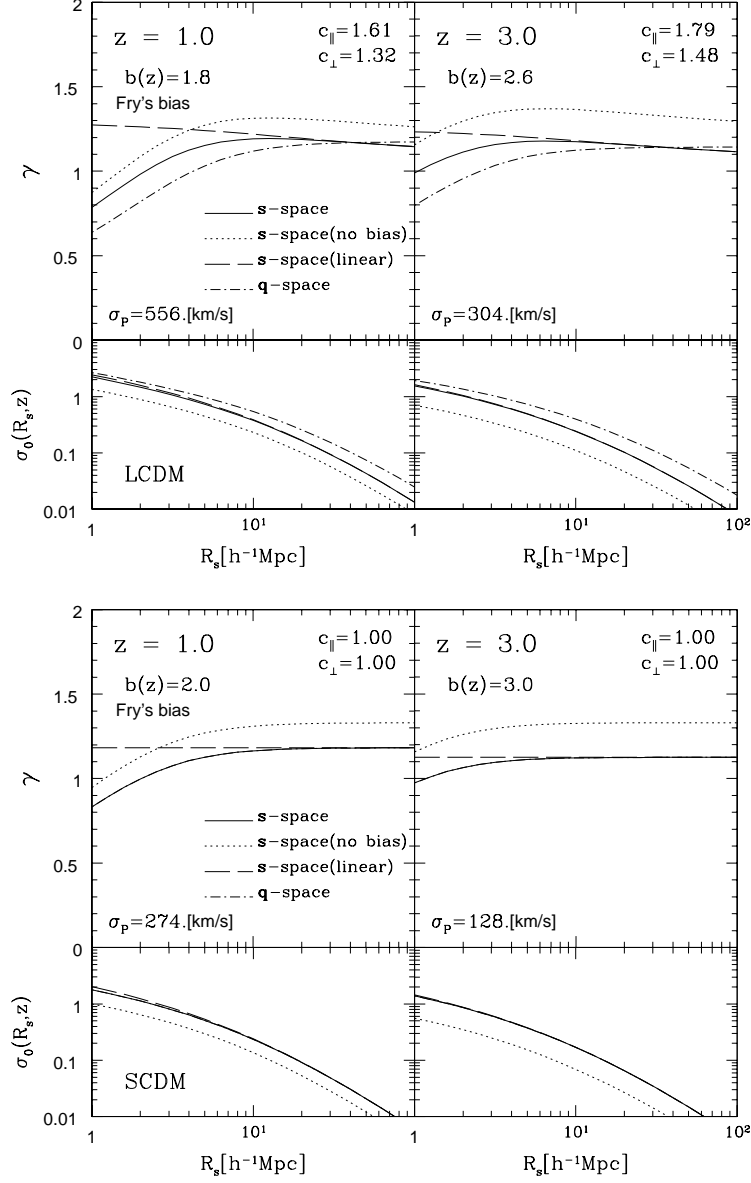


Fig. 4.— Same as Figure 3, but we adopt the cosmological redshift space $s = s_{\text{Ed}}(z)$ (see eqs.[7] and [9]). Note that the SCDM model (the lower panels) is not affected by the geometric distortion because the cosmological redshift-space is exactly same as the real space. Therefore the solid lines exactly coincide with the dot-dashed lines in the SCDM model.

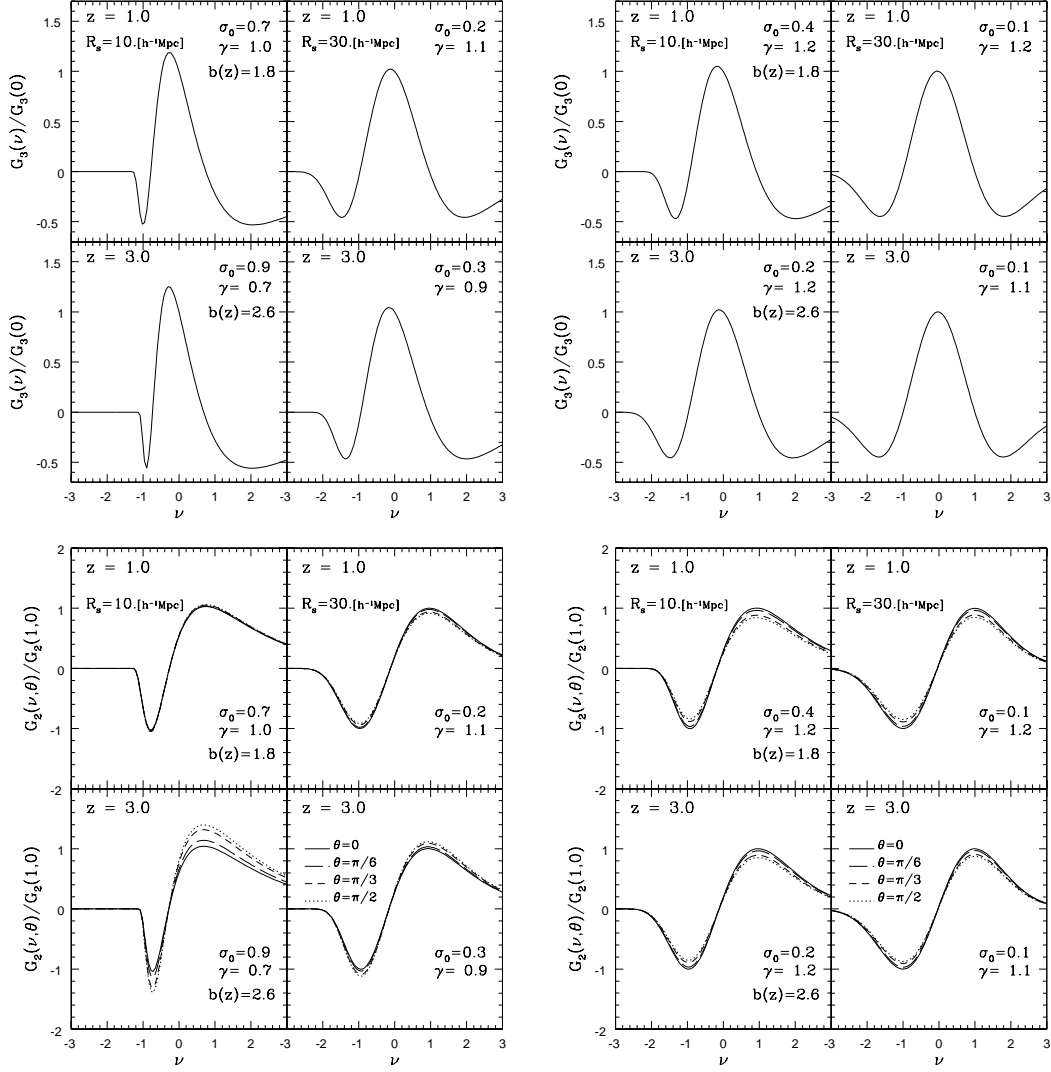


Fig. 5.— Shapes of the isodensity statistics as the function of the density height ν in the LCDM model. We assume the cosmological redshift space $s = s_{\text{Hb}}(z)$ in left-panel, and $s = s_{\text{Ed}}(z)$ in right-panel. In each panel, we show the result with the redshift and the smoothing scale fixed as $z = 1$ and $R_s = 10h^{-1}\text{Mpc}$ (upper-left), $z = 1$ and $R_s = 30h^{-1}\text{Mpc}$ (upper-right), $z = 3$ and $R_s = 10h^{-1}\text{Mpc}$ (lower-left), and $z = 3$ and $R_s = 30h^{-1}\text{Mpc}$ (lower-right). As for the biasing parameter, we adopt the Fry’s bias model with the present value $b_0 = 1.5$: the three-dimensional genus G_3 (*Upper*); the two-dimensional genus G_2 (*Lower*). For G_2 , we plot the cases $\theta = 0$ (solid), $\pi/6$ (long-dashed), $\pi/3$ (short-dashed), and $\pi/2$ (dotted).

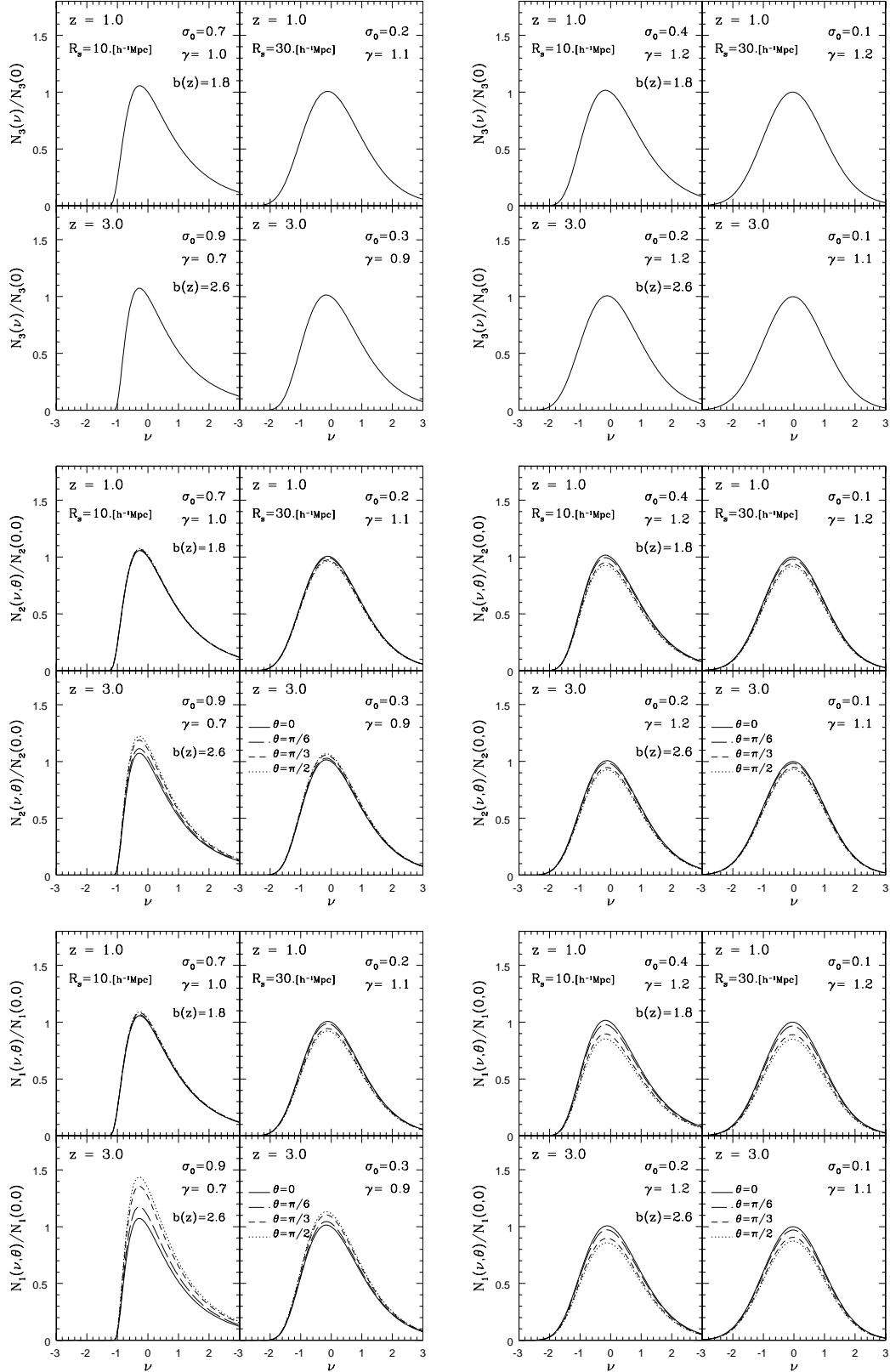


Fig. 6.— Same as Figure 5, but we plot the mean area of isodensity contour N_3 (*Upper*), the mean length of isodensity contour intersecting with a plane N_2 (*Middle*), and the mean number of crossing points of isodensity contour on a line N_1 (*Lower*). For N_2 and N_1 , we plot the cases $\theta = 0$,

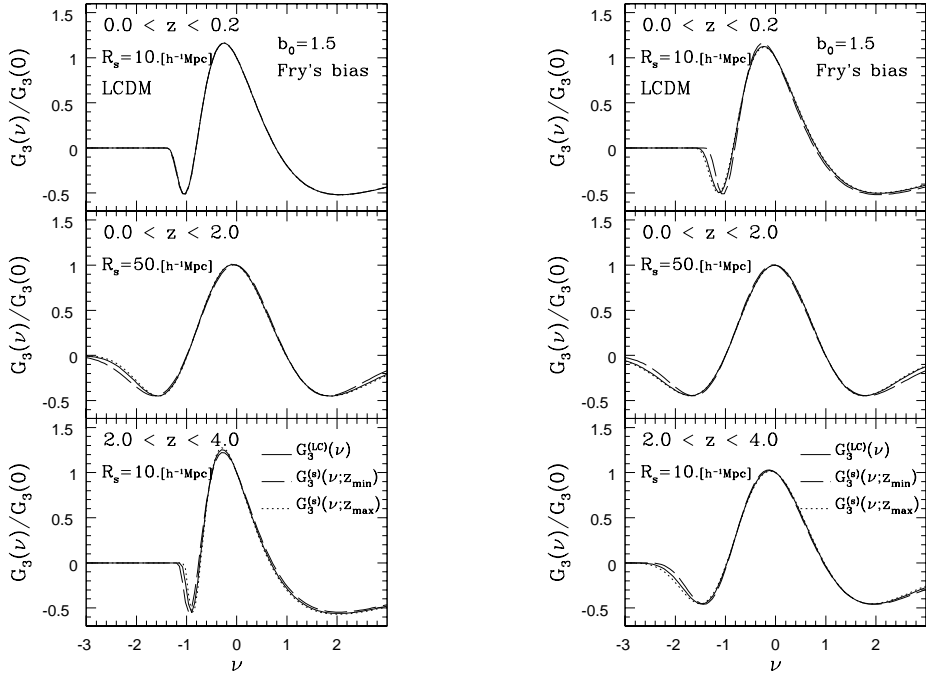


Fig. 7.— The three-dimensional genus curves G_3 evaluated on a light-cone in the LCDM model. For each panel, the evolution of bias is assumed to be the Fry’s model with $b_0 = 1.5$. The cosmological redshift space is chosen as $s = s_{\text{Hb}}(z)$ in left-panel and $s = s_{\text{Ed}}(z)$ in right-panel. The adopted range of the redshift-integration and the smoothing scale are shown in each panel.

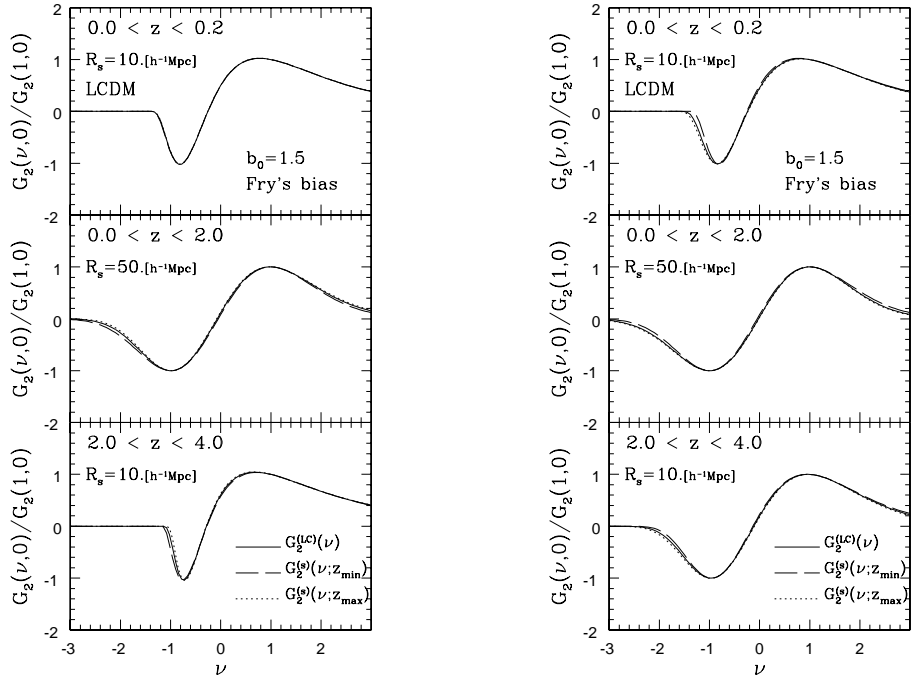


Fig. 8.— Same as Figure 7, but the two-dimensional genus curves G_2 evaluated on a light-cone. Here, we take the two-dimensional slice S parallel to the line-of-sight direction, i.e., $\theta = 0$.